Stochastic Dynamics for Large Deviations and Long-memory in One-dimensional Defect Turbulence

Stochastic Dynamics for Large Deviations and Long-memory in One-dimensional Defect Turbulence

Graduate School of Systems and Engineering

University of Tsukuba

July 2014

Yusuke Uchiyama

Abstract

This dissertation considers defect turbulence of the one-dimensional complex Ginzburg-Landau equation (CGLE). To begin with, a short review of the CGLE is given. Then stochastic models for large deviations and long-memory are introduced for statistical analysis of the defect turbulence. In many previous works, the defect turbulence is regarded as a many body interaction among the Bekki-Nozaki holes and shocks like waves and then is analyzed with some probability distributions. Nonetheless, this picture is not appropriate for the defect turbulence, since there are complicated spatial configurations among localized waves. The identification of localized waves with the use of only amplitude leads to erroneous results. Thus, a new identification method with the use of both amplitude and phase, from the context of *coherent structures*, which is the form of localized traveling waves, is proposed for an appropriate statistical analysis, and gives "local structures". In this case, a defect, a hole, and a modulated amplitude wave are identified as the local structures. With the discrimination, the defect turbulence is described as a birth-death process of the local structures on the basis of a non-stationary master equation describing the probability distribution for number of the three local structures. The three marginal probability distributions for the number of each local structure at the steady state are derived to have the Poisson distribution, which agrees with those of our numerical simulation. In addition, the probability distributions for interarrival time and lifetime of the local structures reproduce successfully the related probability distributions of our numerical simulation based on the marginal time-dependent probability distributions derived from the non-stationary master equation with long-memory. Further, tracing the holes and investigating their kinetics in the defect turbulence are carried out. Some holes show motions affected by acceleration and/or deceleration in contradiction to that a localized wave travels with a constant velocity. Without discrimination of the holes, all the hole velocities are regarded as hole velocity fluctuation in a time series, of which stationary probability density and autocorrelation coefficients display fat tails. It is shown that these characteristics are modeled by generalized Cauchy processes with two generalizations describing the effect of long-memory: a non-autonomous generalized Cauchy process, and a fractional generalized Cauchy process.

Contents

Chapter 1

Introduction

1.1 Background

The world where we live exhibits abundant rich pattern formations in various fields. When we look up to the sky, flowing clouds change their shapes from hour to hour depending on climates, seasons, and so on. Fishes and animals show us beautiful patterns on their skin such as regular stripe patterns of zebras, complicated labyrinth patterns of chub mackerels, and self-similar triangle patterns of cone shells. Our body is also a result from pattern formations. Zygote is firstly a simply monotonous shape, begins to split one after another, and then leads to our complicated body.

The systems showing such patterns are known as nonequilibrium open systems, where energy and/or matter fluxes are sustained [1, 2]. In general, evolution equations describing nonequilibrium open systems are described by nonlinear partial differential equations. It is thus desperate to obtain analytical solution of the evolution equations. However, advances of computer performance in the last few decades have made this research area progress rapidly. Indeed, we can observe unpredictable fascinating pattern formations by carrying out computer simulations.

Spatially complicated and temporally stationary patterns, which can be seen on animal's skin, are results from balances between dissipation and nonlinearity of the evolution equations. On the other hand, subtle disturbance to the system can lead to spatiotemporally chaotic pattern dynamics, which cannot be understand by the language of well-known chaos theory. Such structural instability in terms of intrinsic parameters or disturbance makes it hard to study the systems by conventional mathematical and physical methods having been developed involved in low-dimensional, linear, and deterministic systems. Furthermore, it is quite difficult to establish universal laws for different nonlinear partial differential equations in spite of the specific form of the evolution equations strongly depends on the systems investigated.

Amazingly, we can see common pattern formations in the whole nonequilibrium open systems. In particular, topological defect, which is defined by phase singularity, is one of the most important patterns because it determines qualitative, sometimes quantitative, behavior of the systems. Topological defects have been observed in diverse systems in each dimension: thermal fluid convection in closed loop shows one-dimensional (1D) defect dynamics [3, 4]; two-dimensional (2D) systems especially provide abundant examples of topological defects such as chemical reactions [5, 6], liquid crystals [7, 8], heart tissues [9, 10, 11], and so on; historically, there-dimensional (3D) defect is

the most famous, namely, vortex in fluids [12].

In order to extract the common nature without directly dealing with original evolution equations, mathematical techniques, the method of multiple scales [13, 14] and the reductive perturbation method [15], have been developed. These methods allow us to investigate nonequiribrium open systems by an evolution equation with respect to a complex field describing slow amplitude modulation near a Hopf bifurcation. In particular for a primary supercritical Hopf bifurcation, the evolution equation is given by the complex Ginzbrug-Landau equation (CGLE) [1, 16, 17].

The CGLE can also present defect dynamics observed in various nonequilibrium open systems in several dimensions and thus can be regarded as a normal form in the systems. This means that we can understand the nature of nonequilibrium open systems through the CGLE qualitatively, sometimes quantitatively. From this point of view, we study pattern formations of the CGLE in this dissertation. Historically, the CGLE has been utilized as a phenomenological model for investigating birth-death processes of topological defects especially in 2D systems. As far as we know, the first attempt is that the birth-death process of topological defects of the two-component 2D CGLE can be explained by the master equation involved in a pair-extinction process giving a sub-Poisson statistics as the modified Poisson distribution [18]. With the help of this notion, topological defect turbulence in a catalytic surface reaction has been investigated [19]. Furthermore, traveling topological defects in inclined layer convection has been associated with the 2D CGLE and their number statistics has been obtained from the birth-death process with the squared Poisson distribution. While these birth-death processes give physical explanations to the systems, the consistent theory for the number statistics with other index, such as correlations, has yet to be established.

1.2 Purpose and Outline

The purpose of this dissertation is to develop a methodology for analyzing spatiotemporally chaotic dynamics involved in phase singularity in nonequilibrium open systems. From the point of view of risk analysis for human hearts, phase singularity plays an important role. Our heart shows nearly regular pacing with the noise having a fractal nature in ordinary states. However, when we have a heart disease, the beat rhythm turns into irregular pacing. In particular under ventricular fibrillation, which leads to sudden death, an electric field on a human heart displays chaotic dynamics of phase singularity with annihilation and creation of phase singularities [21]. Recently, other type of phase singularity was observed in a healthy human heart and was identified by the Bekki-Nozaki hole, which is an exact solution of the 1D CGLE [22]. Nonetheless, the appropriate methodology for analyzing the dynamics in complex configurations with multiple-waves in each dimension has yet to be established. Therefore, for the first step of this grandiose project, we focus on the 1D CGLE and then try to develop new strict methods for analyzing the spatiotemporally dynamics by means of stochastic dynamical model in detail. To the best of our knowledge, such an attempt has yet to be done for the CGLE in each dimension.

This dissertation is consisted of seven chapters, and is organized as follows.

In Chapter 2, a short review of the CGLE is given. The CGLE has been introduced by the method of multiple scales or the reductive perturbation method near a supercritical Hopf bifurcation and then can describe slow amplitude modulation with respect to time and space. It is thus expected to have common nature in oscillatory media. Indeed, it exhibits defect dynamics, which is dynamical

behavior of phase singularity, in one, two, and three-dimensions such as the BN-hole, spiral wave, and vortex filament. In particular in 1D systems, localized nonlinear waves have been extensively investigated in the context of *coherent structures* having the form of a traveling wave with constant velocity in oscillatory background. In addition, several spatiotemporal dynamics of the CGEL have been observed by computer simulation. Some results from statistical analysis in 2D systems have also been reported especially for defect number.

In Chapter 3, mathematical tools for modeling stochastic dynamics in spatiotemporally chaotic dynamics of the CGEL are introduced. The key concept of them is how to describe large deviations and long-memory. One of the simplest models for large deviations is a generalized Cauchy process, of which stationary distribution is a generalized Cauchy distribution having fat tails. Master equation is known to describe a stochastic dynamics with respect to state transitions. There are two ways in modeling long-memory for a master equation: a non-stationary master equation and a generalized master equation. Both master equations lead to the corresponding Fokker-Planck equations, which give evolutions of probability density functions (PDFs) for continuous states, with their representations of random variables by the Kramers-Moyal expansion.

In Chapter 4, statistical analysis for "defect turbulence", which is a state of spatiotemporal high-dimensional chaos involved in phase singularity, is carried out naively based on interactions between the local depressing waves (LDWs) and local standing waves (LSWs). Three statistics for LDW are presented: LDW number, inter-LDWs distance, and depth of LDW. The fluctuation of LDW number is subjected to a sub-Poisson statistics, which implies the existence of LDWs bunching states. Indeed, nearest neighbor interactions between LDWs are recognized in the probability distribution for inter-LDWs distance. On the other hand, the probability distribution except the existence of the LDWs bunching states is modeled by a Poisson configuration with a fluctuating parameter. Depth of LDW shows the existence of long-range interactions, which can be modeled by a space-time fractional Poisson process.

In Chapter 5, it is elucidated that the defect turbulence is a birth-death process of defects, holes, and modulated amplitude waves (MAWs), which are localized nonlinear waves being "key players of the game". This is the main result of this dissertation. Appropriate discrimination methods of the local structures are developed with the use of both local amplitude and phase, and then give a master equation under their interaction scheme. In this case, the master equation gives the probability distributions for number of defect, hole, and MAW as the Poisson distribution at the steady state. On the other hand, the probability distributions for interarrival time of defects, lifetime of holes, and that of MAWs show the existence of long-memory and the peaks due to collective motions. A non-stationary master equation, as a generalization of the master equation, provides evolution of the marginal Poisson distributions of the three local structures and the interarrival (and lifetime) distributions with the long-memory and the peaks consistently.

In Chapter 6, the kinetics of hole velocity is investigated. Generally speaking, velocity of localized waves is assumed to be constant in various fields. Nevertheless, the holes in the defect turbulence display acceleration and deceleration of their motions, namely hole velocity varies temporally. Collected hole velocities in the whole space without discrimination, successive hole velocities can be regarded as a stochastic process and then show the existence of large deviations and long-memory. These properties are modeled by a stochastic differential equation with a suitable modification for the conventional Fokker-Planck equation.

In Chapter 7, summary of this dissertation and future prospects are presented.

Chapter 2

Short Review of the complex Ginzburg Landau equation

In this chapter, we present a short review of the CGLE especially in 1D systems. The CGLE describes slow amplitude modulation of spatially extended oscillatory fields in nonequilibrium open systems. The CGLE can exhibit defect dynamics in one-, two-, and three-dimensions as behavior of the BN-holes, spiral waves, and vortex filaments, respectively. In particular, the 1D CGLE has been extensively investigated involved in connection with localized nonlinear waves (soliton, the BN-hole, and shock), spatiotemporal dynamics, and statistical analysis.

2.1 Physical background

Pattern formations in nonequilibrium open systems are generally described by the multi-components nonlinear advection reaction diffusion equation:

$$\frac{\partial}{\partial t}\mathbf{U} + \mathbf{v}\cdot\nabla\mathbf{U} = D\nabla^2\mathbf{U} + \mathbf{F}(\mathbf{U},\mu), \tag{2.1}$$

where $\mathbf{U}$ is a field of physical quantity considered, $\mathbf{v}$ is an advection velocity, D is a diffusion coefficients matrix and $\mathbf{F}(\cdot,\mu)$ is a reaction term with an intrinsic parameter μ. A spatially homogeneous steady state $\mathbf{U}^*$, which satisfies the relation $\mathbf{F}(\mathbf{U}^*,\mu) = \mathbf{0}$, gives a Jacobian matrix $\partial\mathbf{F}(\mathbf{U}^*,\mu)/\partial\mathbf{U}$. An eigenvalue problem in terms of the Jacobian matrix gives a set of eigenvalues and eigenvectors $\{\lambda_n(\mu),\mathbf{U}_n(\mu)\}$ depending on μ. When the eigenvalues with a certain value of μ satisfy the condition that only one pair of complex conjugate eigenvalues exists on the imaginary axis and others are in the left plane (Fig. 2.1(a)), such a parameter μ_c is known as a critical value associated with a Hopf bifurcation and is assumed to satisfy $\partial\lambda(\mu_c)/\partial\mu > 0$. Under a perturbation to μ_c as $\mu = \mu_c + \varepsilon$, evolution of $\mathbf{U}$ is described by a slow amplitude modulation $A(\mathbf{x},t)$ with the pair of complex conjugate eigenvalues being on the imaginary axis (Fig. 2.1(b)) and their eigenvectors in terms of μ_c as

$$\mathbf{U} = A(\mathbf{x},t)\mathrm{e}^{\lambda_0(\mu_c)t}\mathbf{U}_0(\mu_c) + c.c., \tag{2.2}$$

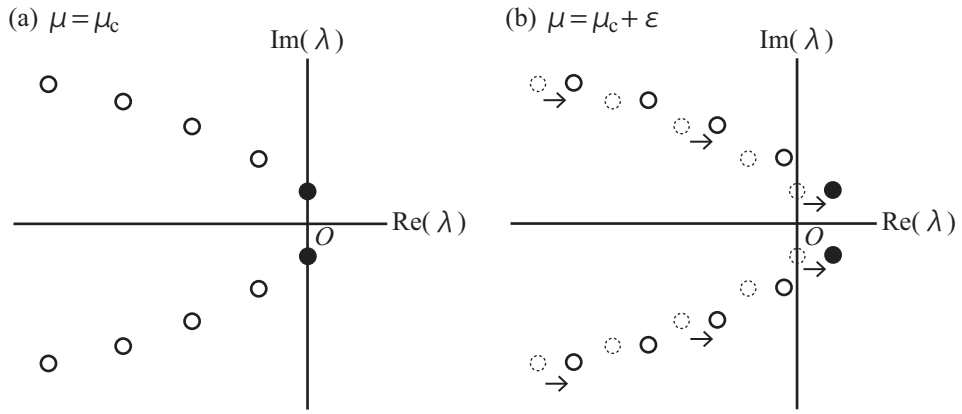

Figure 2.1: Conceptual diagrams of configurations of eigenvalues depending on μ. (a) When $\mu = \mu_c$, one pair of complex conjugate eigenvalues, denoted by black circles, exists on the imaginary axis and others, denoted by white circles, are in the left plane. (b) Under a perturbation to μ_c as $\mu = \mu_c + \varepsilon$, the eigenvalues move to the right plane. Then, the pair of eigenvalues denoted by black circles intersects the imaginary axis and leads to an instability. Such an instability gives a Hopf bifurcation, which is involved to oscillatory media.

where $c.c.$ denotes the complex conjugate term. The evolution equation of $A(\mathbf{x}, t)$ is given by the method of multiple scales [14] or the reductive perturbation method [16] as

$$\frac{\partial}{\partial t}A = A + (1 + ic_1)\nabla^2 A - (1 + ic_2)|A|^2 A \tag{2.3}$$

with the parameters c_1 and c_2 being obtained from the intrinsic parameters of original systems. Depending on the specific values of c_1 and c_2, the CGLE display various pattern formations. It is thus regarded as a normal form of nonequilibrium open systems, especially, oscillatory media [17].

2.2 Defects in several dimensions

2.2.1 The Bekki-Nozaki hole

The CGLE can describe defect dynamics in several dimensions. In homogeneous and infinitely extended 1D systems, a defect solution is analytically obtained by the modified bilinear method [23, 24] as

$$A(x,t) = \frac{b_1 \exp(\kappa\xi) + b_2 \exp(-\kappa\xi)}{\exp(\kappa\xi) + \exp(-\kappa\xi)} \exp[i(qx - \Omega t)] \exp[-i\alpha \ln(2\cosh(\kappa\xi))] \tag{2.4}$$

with ξ being a position on a moving frame with a constant velocity v. The asymptotic wavenumbers, $k_1 = q - \alpha\kappa$ and $k_2 = q + \alpha\kappa$, are related to v by the following form:

$$v = (c_1 - c_2)(k_1 + k_2). \tag{2.5}$$

The amplitude of the asymptotic plane waves b_1 and b_2 satisfy

$$|b_1| = \sqrt{1-k_1^2}, \;\; |b_2| = \sqrt{1-k_2^2} \tag{2.6}$$

with $0 < k_1, k_2 < 1$ and the frequency Ω is given by

$$\Omega = c_1 k_1^2 + \kappa\alpha v + c_2(1-k_1^2) = c_1 k_2^2 + \kappa\alpha v + c_2(1-k_2^2). \tag{2.7}$$

In particular, if the parameter b_1 takes a real value, the parameter b_2 can then be written as $b_2 = |b_2|\exp(i\Phi)$, where

$$\cos\Phi = -\frac{b_1}{|b_1|\eta}[(1+\alpha^2)(1+c_1^2)\kappa^2 - q^2(1+c_2^2)], \tag{2.8}$$

$$\sin\Phi = 4q\kappa a(1+c_1^2)(1+\alpha^2), \tag{2.9}$$

$$\eta = (1+\alpha^2)(1+c_1^2)\kappa^2 - 2q\kappa a(1+c_1^2)(1+\alpha^2) + q^2(1+c_2^2). \tag{2.10}$$

The parameter α, which is introduced in the form of the modified bilinear operator, and the negative a are determined by the following relations:

$$\alpha = -\beta \pm \sqrt{2+\beta^2}, \;\; \beta = \frac{3(1+c_1c_2)}{2(c_2-c_1)}, \;\; a = \frac{c_1-c_2}{3\alpha(1+c_1^2)}. \tag{2.11}$$

The two asymptotic wavenumbers k_1 and k_2 lay on an ellipse as

$$\frac{(k_1+k_2)^2}{a_1^2} + \frac{(k_1-k_2)^2}{a_2^2} = 1, \tag{2.12}$$

where

$$a_1^2 = 4\left[1 - \frac{1+c_2^2}{a(1+\alpha^2)(1+c_1)^2}\right]^{-1}, \;\; a_2^2 = 4\left(1 - \frac{1}{a\alpha^2}\right)^{-1}. \tag{2.13}$$

This is the specific form of the BN-hole, which connects two plane waves with different wavenumbers and then has phase singularity in its core. Figure 2.2 shows amplitude and phase profile of the BN-hole. One can recognize a phase jump in the core characterized by an amplitude dip. Stability analysis with a weak perturbation shows that the BN-hole is structualy unstable [25].

2.2.2 Spiral wave

Spiral wave, of which core is phase singularity, plays as a defect in 2D systems. The analytical form of an isolated spiral wave in the polar coordinate (r, θ) is given by

$$A(r,\theta,t) = \rho(r)\exp[i(m\theta - \omega t + \psi(r))], \tag{2.14}$$

where m is the winding number, ω is the rotation frequency of the spiral wave, $\rho(r)$ is the amplitude, and $\psi(r)$ is the phase [26]. This form is obtained by a perturbation method under the boundary conditions:

$$\rho(r) \sim r^m \;\; (r \to 0), \;\; \partial_r\psi(0) = 0, \tag{2.15}$$

$$\rho(r), \partial_r\psi(r) < \infty \;\; (r \to \infty). \tag{2.16}$$

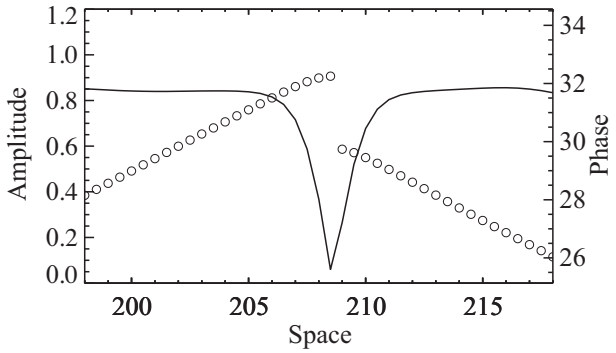

Figure 2.2: Amplitude and phase profile of the BN-hole. Solid line denotes amplitude, and white circles denote phase.

The winding number m corresponds to the arm number of the spiral wave, and if and only if $m = \pm 1$, the spiral wave is stable. The instability among $m \neq \pm 1$ induces breakup of the spiral wave, which can be often observed in real situations of chemistry and physiology. Figure 2.3 shows stationary spiral waves in phase field obtained by a numerical simulation. There are both clockwise and counterclockwise rotating spiral waves associated with the sign of the winding numbers. The tip of each spiral wave corresponds to the phase singularity.

2.2.3 Vortex filament

In 3D systems, phase singularity appears as a line, which is the core of a scroll wave. A scroll wave in the cylindrical coordinates (r, θ, z) is of the form:

$$A(r, \theta, z, t) = \rho(r)\exp[i(m\theta - \omega t + \psi(r) + k_z z)], \tag{2.17}$$

where k_z is an axial wave number characterizing a twist [27]. The motion of an isolated vortex filament was investigated by a phenomenological equation describing its velocity kinetics. With the assumption that a vortex filament is as almost straight as paralleling to axis z, the velocity kinetics is given by

$$\partial_t \mathbf{v} + \hat{K}(c_1^{-1}\mathbf{v} - \partial_z \mathbf{r}) = \mathbf{0}, \tag{2.18}$$

where $\mathbf{r}$ is a position along the vortex filament characterized by the z coordinate, and $\hat{K}$ is the friction tensor of which components are real and symmetric. Vortex filaments appear in various dynamics with the value sets of the parameters of the CGLE: an isolated vortex filament, a closed loop of a vortex filament, and nucleation and collapse of vortex filaments.

2.3 Localized nonlinear waves

In 1D systems, a form of localized waves on a moving frame, called *coherent structures*, has been introduced [28]. Substituting the ansatz $A(x, t) = \hat{A}(\xi)\mathrm{e}^{-i\omega t}$ with $\xi = x - vt$ into the 1D CGLE,

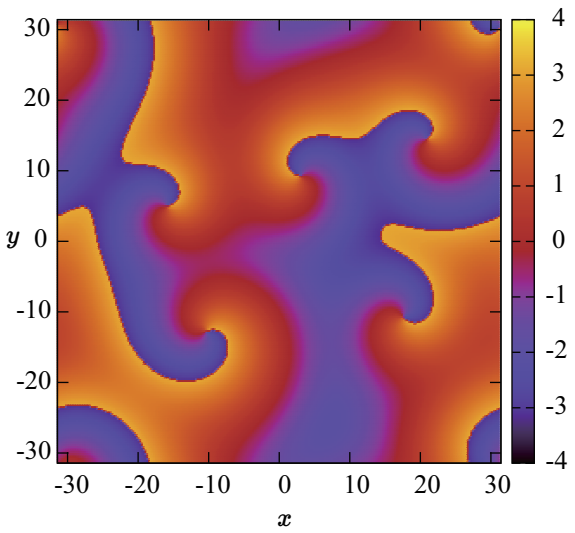

Figure 2.3: Stationary spiral waves in phase field. There are both clockwise and counterclockwise rotating spiral waves associated with the sign of the winding numbers. The tip of each spiral wave corresponds to the phase singularity.

one obtains the ordinary differential equations:

$$\frac{\mathrm{d}}{\mathrm{d}\xi}a = \kappa a, \tag{2.19a}$$

$$\frac{\mathrm{d}}{\mathrm{d}\xi}\kappa = -\frac{1+c_1\omega}{1+c_1^2} - \frac{v}{1+c_1^2}\kappa - \frac{c_1 v}{1+c_1^2}q + \frac{1+c_1c_2}{1+c_1^2}a^2 - \kappa^2 + q^2, \tag{2.19b}$$

$$\frac{\mathrm{d}}{\mathrm{d}\xi}q = \frac{c_1-\omega}{1+c_1^2} + \frac{c_1 v}{1+c_1^2}\kappa - \frac{v}{1+c_1^2}q + \frac{c_2-c_1}{1+c_1^2}a^2 - 2\kappa q, \tag{2.19c}$$

where v is a velocity on the frame, ω is a frequency of background, and the variables $(a(\xi), \kappa(\xi), q(\xi))$ are, respectively, defined by $a = |\hat{A}(\xi)|$ and $\kappa + iq = \mathrm{d}\ln A/\mathrm{d}\xi$. The coherent structures appear as fixed points or closed orbits in the three dimensional dynamical systems: plane wave is a stable fixed point, the BN-hole and the shock are heteroclinic orbits connecting two plane waves with different wave numbers.

Subsequently, the two different homoclinic orbits were discovered: homoclinic hole [29], and modulated amplitude wave (MAW) [30]. They, respectively, correspond to an unstable and a stable brunch of a homoclinic orbit associated with a saddle-node bifurcation. The amplitude profile of a homoclinic hole is quite similar to that of the BN-hole, however, the phase profiles of them show different features as shown in Fig. 2.4. The phase of a homoclinic hole has no singularity because it connects the same plane wave as a homoclinic orbit. The amplitude profile of an MAW is characterized by weak modulation rather than a homoclinic hole.

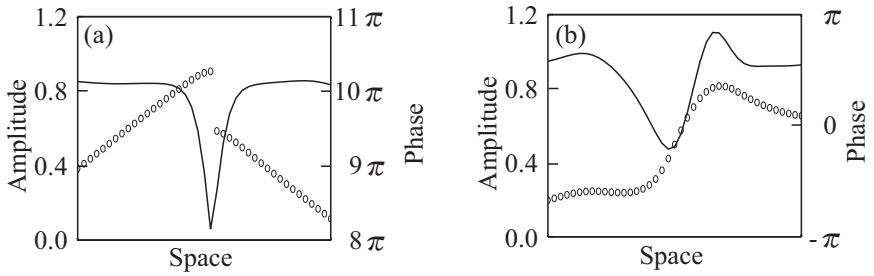

Figure 2.4: Amplitude and phase profiles of (a) the BN-hole and (b) a homoclinic hole. The amplitude profile of both hole have localized dips. The phase of the BN-hole jumps at the core of the amplitude whereas that of the homoclinic hole is continuous.

2.4 Spatiotemporal dynamics

In addition to the isolated localized waves, spatiotemporal dynamics of the 1D CGLE has been investigated. Chaté reported a phase diagram of the parameter $(c_1, -c_2^{-1})$ classifying various spatiotemporal dynamics by extensive numerical simulations [31]. According to his phase diagram, of which a modification is shown in Fig. 2.5, one can observe two spatiotemporally chaotic dynamics, phase turbulence and defect turbulence.

In the phase turbulence, many MAW-like ripples display creation and annihilation process among themselves. Then the transition from a propagating single MAW to the phase turbulence is considered to result from sequential saddle node bifurcations. The defect turbulence displays chaotic behavior on both amplitude and phase. A road to the defect turbulence was investigated to be caused by splitting processes of the BN-hole like waves [32].

Based on the nearest neighbor interactions between localized nonlinear waves, some spatiotemporal dynamics can be mimicked. To mimic the spatiotemporal dynamics classified into spatiotemporal intermittency, van Hecke introduced a coupled map lattice describing phase dynamics involved in the BN-hole like and homoclinic like localized waves [33]. According to his work, we call a BN-hole like and a homoclinic hole like waves as a defect and a hole, respectively. The coupled map lattice gives a significant insight that defects and holes are key players in the regime of the spatiotemporal intermittency.

2.5 Statistical analysis

In physics, many degrees of freedom chaotic states, such as turbulence in fluid, have been often studied by computational and/or statistical methods. For the CGLE in several dimensions, some results of spatiotemporal chaos obtained by statistical analysis have been reported.

Sakaguchi investigated soliton turbulence in the 1D CGLE at a dispersion limit, where soliton-like pules can be observed because the system is regarded as the nonlinear Schrödinger equation with weak perturbations [34]. Then, he obtained the stationary probability distributions for amplitudes and wave numbers of the soliton-like pulses, and concluded that the soliton turbulence is an one-parameter family spatiotemporal dynamics. Wang introduced an external white noise into the 2D

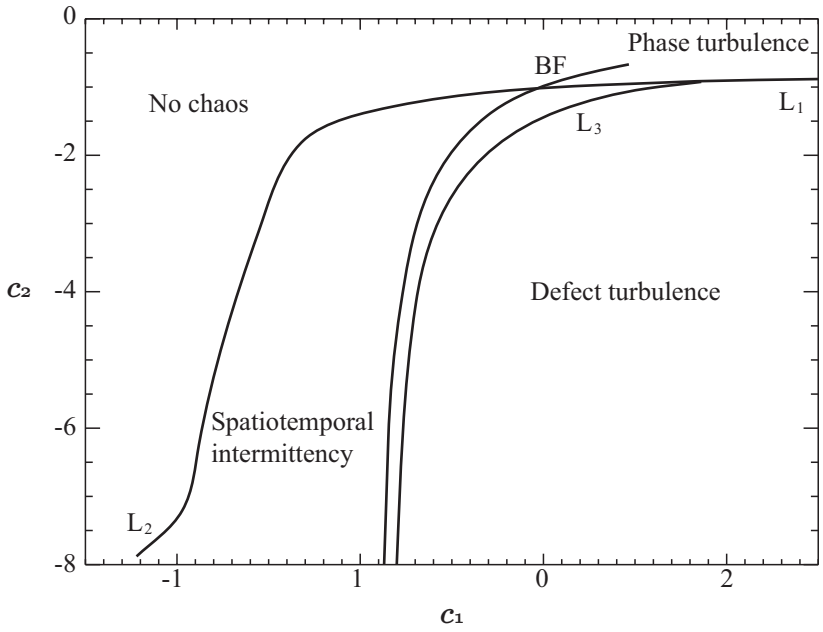

Figure 2.5: The phase diagram of the 1D CGLE cited from Ref. [31]. The parameters b_1 and b_3 correspond to c_1 and $-c_2^{-1}$, respectively.

CGLE and showed that the noise intensity changes the shape of probability distributions for defect number [35]. This is an example of the realization of stochastic bifurcation [36]. Daniels *et al*. revealed that defect velocity fluctuation of the 2D CGLE has fat tails in its stationary probability distribution [37]. This means that the defects do not behave as Brownian particles.

2.6 Summary

The CGLE is derived from evolution equations in nonequilibrium open systems by the method of multiple scales or the reductive perturbation method. One can observe defects in each dimension since the CGLE is a normal form of spatially extended systems with dissipations and oscillations. In particular, localized nonlinear waves in 1D systems is classified as the coherent structures, and have been extensively investigated their dynamics. Furthermore, spatiotemporal, especially chaotic, dynamics have been recognized in the 1D systems with the corresponding phase diagram on the parameters of the CGLE. Some statistical analysis have been carried out in order to understand the features of spatiotemporally chaotic dynamics in many degrees of freedom.

Chapter 3

Stochastic models for large deviations and long-memory

In this chapter, we introduce stochastic models for large deviations and long-memory. To begin with, we present a generalized Cauchy process, of which PDF can describe large deviations. Subsequently, we show that the effect of long-memory can be incorporated into a master equation by two ways: a non-stationary master equation, and a generalized master equation. The Kramers-Moyal expansion of them gives the corresponding Fokker-Planck equations with the realizations of sample paths.

3.1 Generalized Cauchy process

Large deviations in many systems are associated with the occurrence of rare events, disaster, and hazard far from standard statistical law being subjected to the Gaussian distribution. The corresponding probability distributions are conventionally given by alpha-stable distributions, especially, the Cauchy distribution for $\alpha = 1$ [38]. One generalization of the Cauchy distribution, known as a generalized Cauchy distribution, has been extensively studied associated with various complex systems [39, 40, 41].

There are many stochastic processes having the generalized Cauchy distribution as their stationary probability distribution. One candidate of them is an Itô type stochastic differential equation (SDE) [42, 43], which is known as a generalized Cauchy process (GCP) consist of a linear dissipation, an additive and a multiplicative standard Brownian motion. The GCP is given in the form:

$$\mathrm{d}X(t) = -\gamma X(t)\mathrm{d}t + \sqrt{2D_m}X(t)\mathrm{d}W_m(t) + \sqrt{2D_a}\mathrm{d}W_a(t), \tag{3.1}$$

with $W_m(t)$ and $W_a(t)$ being the standard Brownian motions, and positive real parameters γ, D_a and D_m. The analytical solution of Eq. (3.1) is explicitly given by the Itô stochastic integral [42, 43] as

$$X(t) = X(0)\mathrm{e}^{-\gamma t+\sqrt{2D_m}W_m(t)} + \sqrt{2D_a}\int_0^t \mathrm{e}^{\gamma(t'-t)-\sqrt{2D_m}[W_m(t')-W_m(t)]}\mathrm{d}W_a(t'). \tag{3.2}$$

The autocorrelation function, defined by $C(t) = \langle X(t)X(0)\rangle$, is obtained as

$$C(t) = \langle X(0)^2\rangle\langle \mathrm{e}^{-\gamma t+\sqrt{2D_m}W_m(t)}\rangle, \tag{3.3}$$

where $\langle\cdots\rangle$ denotes an ensemble average.

The corresponding Fokker-Planck equation is given by

$$\frac{\partial}{\partial t}P(x,t) = \frac{\partial}{\partial x}[\gamma x P(x,t)] + \frac{\partial^2}{\partial x^2}[(D_m x^2 + D_a)P(x,t)]. \tag{3.4}$$

Under the stationary state, $\partial_t P(x,t) = 0$, the stationary distribution $P_s(x)$ is readily obtained as

$$P_s(x) = \frac{a^{2b-1}}{B(b-1/2,1/2)}\frac{1}{(x^2+a^2)^b}, \tag{3.5}$$

where $B(\cdot,\cdot)$ is the beta function, the parameters a and b are defined by

$$a = \sqrt{\frac{D_a}{D_m}}, \quad b = 1 + \frac{\gamma}{2D_m}. \tag{3.6}$$

The stationary distribution in Eq. (3.5) is the generalized Cauchy distribution. The even number order moments with respect to $P_s(x)$ exist with certain parameter values due to the symmetry of $P_s(x)$. In particular, the second order moment is expressed by

$$\langle X^2\rangle_s = \frac{D_a}{2(\gamma - D_m)}, \tag{3.7}$$

when $\gamma > D_m$ is satisfied. This relation, with the help of the Bloch's theorem given in Appendix A, provides the specific form of the autocorrelation function $C(t)$ in Eq. (3.3) as

$$C(t) = \frac{D_a}{2(\gamma - D_m)}\mathrm{e}^{-(\gamma - D_m)t}. \tag{3.8}$$

3.2 Master equations with long-memory

A conventional master equation provides evolution of a probability distribution with respect to states of a particle [42, 43]. This evolution equation is derived from state transition rules on particle systems as

$$\frac{\mathrm{d}}{\mathrm{d}t}P(\mathbf{r},t) = \sum_{\mathbf{r}'}[w(\mathbf{r},\mathbf{r}')P(\mathbf{r}',t) - w(\mathbf{r}',\mathbf{r})P(\mathbf{r},t)] \tag{3.9}$$

with particle states $\mathbf{r}$, and transition probabilities $w(\mathbf{r},\mathbf{r}')$ on $\mathbf{r}'\to\mathbf{r}$ being constrained that $\sum_{\mathbf{r}'} w(\mathbf{r},\mathbf{r}') = 1$. The master equation has Markov property, namely the probability distribution at each time is only affected by the one of infinitessimal previous time.

On the other hand, stochastic dynamics in complex systems often shows the existence of long-memory, which presents non-Markov property. There are two ways in generalizing master equations to have non-Markov property: one is a non-stationary master equation [44, 45], the other is a generalized master equation [46, 47, 48].

A non-stationary master equation,

$$\begin{aligned}\frac{\mathrm{d}}{\mathrm{d}t}P(\mathbf{r},t) &= \sum_{\mathbf{r}'}[w(\mathbf{r},\mathbf{r}',t)P(\mathbf{r}',t) - w(\mathbf{r}',\mathbf{r},t)P(\mathbf{r},t)] \\ &= \nu(t)\sum_{\mathbf{r}'}[\tilde{w}(\mathbf{r},\mathbf{r}')P(\mathbf{r}',t) - \tilde{w}(\mathbf{r}',\mathbf{r})P(\mathbf{r},t)], \end{aligned} \tag{3.10}$$

is characterized by time-dependent transition probabilities having the form $w(\mathbf{r},\mathbf{r}',t) = \nu(t)\tilde{w}(\mathbf{r},\mathbf{r}')$. A time-scaling function $\nu(t)$ has to be non-negative. When $\nu(t)$ satisfy the condition that $\lim_{t\to\infty}\nu(t) = 0$, the solution of Eq. (3.10) can describe the effect of long-memory. Indeed, the following functions satisfy this condition:

$$\frac{n\nu_0 t^{n-1}}{1+\nu_1 t^n}\ (\nu_0,\nu_1>0), \quad t^\alpha\ (0<\alpha<1). \tag{3.11}$$

Introduced the rescaled time $\tilde{t} = \int_0^t \nu(t')\mathrm{d}t'$, Eq. (3.10) leads to a conventional master equation with respect to $\tilde{t}$ as,

$$\frac{\mathrm{d}}{\mathrm{d}\tilde{t}}P(\mathbf{r},\tilde{t}) = \sum_{\mathbf{r}'}[\tilde{w}(\mathbf{r},\mathbf{r}')P(\mathbf{r}',\tilde{t}) - \tilde{w}(\mathbf{r}',\mathbf{r})P(\mathbf{r},\tilde{t})]. \tag{3.12}$$

Thus, the solution of the conventional master equation readily gives that of the corresponding non-stationary master equation.

A generalized mater equation has been introduced in the context of continuous time random walks (CTRWs), where duration time between state transitions is subjected to a waiting time distribution. The generalized master equation can express the effect of long-memory by a convolution with a memory functions as

$$\frac{\mathrm{d}}{\mathrm{d}t}P(\mathbf{r},t) = \frac{\mathrm{d}}{\mathrm{d}t}\int_0^t \mathrm{d}t' M(t-t')\sum_{\mathbf{r}'}[w(\mathbf{r},\mathbf{r}')P(\mathbf{r}',t') - w(\mathbf{r}',\mathbf{r})P(\mathbf{r},t')], \tag{3.13}$$

where the Laplace transform of the memory function $M(t)$ is associated with that of a waiting time distributions $\psi(t)$ by

$$\hat{M}(s) = \frac{\hat{\psi}(s)}{1-\hat{\psi}(s)}, \tag{3.14}$$

where the hat symbol denotes the Laplace transform.

When the waiting time distribution is subjected to a power-law at large t as $\psi(t)\sim t^{-1-\alpha}$ $(0<\alpha<1)$, the memory function has the same property as $M(t)\sim t^{-\alpha}$. The corresponding generalized master equation is expressed as

$$\frac{\mathrm{d}}{\mathrm{d}t}P(\mathbf{r},t) = {}_0\mathbf{D}_t^{1-\alpha}\sum_{\mathbf{r}'}[w(\mathbf{r},\mathbf{r}')P(\mathbf{r}',t) - w(\mathbf{r}',\mathbf{r})P(\mathbf{r},t)], \tag{3.15}$$

where the operator ${}_0\mathbf{D}_t$ is the Riemann-Liouville fractional derivative [49] defined by

$${}_0\mathbf{D}_t^{1-\alpha}f(t) = \frac{1}{\Gamma(\alpha)}\frac{\mathrm{d}}{\mathrm{d}t}\int_0^t (t-t')^{\alpha-1}f(t')\mathrm{d}t' \tag{3.16}$$

with $\Gamma(\cdot)$ being the gamma function. This master equation is known as a fractional master equation.

3.3 The Fokker-Planck equations with long-memory

Master equations can also describe continuous states by the assumption that a state $\mathbf{r}$ is a representative state in a partitioned region of which volume is V. This procedure for right hand side of a master equation leads to

$$L_{ME}P(\mathbf{r},t) = \int_V [w(\mathbf{r},\mathbf{r}')P(\mathbf{r}',t) - w(\mathbf{r}',\mathbf{r})P(\mathbf{r},t)]\mathrm{d}\mathbf{r}'. \tag{3.17}$$

Here L_{ME} denotes a linear operator describing the right hand side of conventional, non-stationary, and generalized master equations.

The Taylor series of Eq. (3.17) with respect to the infinitesimal variation defined by $\delta\mathbf{r} = \mathbf{r} - \mathbf{r}'$ gives

$$L_{ME}P(\mathbf{r},t) = \int_V \mathrm{d}\delta\mathbf{r} \sum_{m=1}^{\infty} \frac{(-1)^m}{m!} \left(\sum_{k=1}^{n} \delta x_k \frac{\partial}{\partial x_k} \right)^m w(\mathbf{r}'+\delta\mathbf{r},\mathbf{r})P(\mathbf{r},t). \tag{3.18}$$

This procedure is known as the Kramers-Moyal expansion [42]. By terminating the series at the second term and replacing

$$F_i(\mathbf{r}) = \int_V \delta x_i w(\mathbf{r}'+\delta\mathbf{r},\mathbf{r})\delta\mathbf{r}, \quad D_{ij}(\mathbf{r}) = \int_V \delta x_i \delta x_j w(\mathbf{r}'+\delta\mathbf{r},\mathbf{r})\delta\mathbf{r}, \tag{3.19}$$

one obtains the Fokker-Planck operator defined by

$$L_{FP}P(\mathbf{r},t) = \left[\sum_{i=1}^{n} \frac{\partial}{\partial x_i} F_i(\mathbf{r}) + \frac{1}{2} \sum_{i,j=1}^{n} \frac{\partial^2}{\partial x_i \partial x_j} D_{ij}(\mathbf{r}) \right] P(\mathbf{r},t). \tag{3.20}$$

In addition, the corresponding Itô-type SDEs are presented by

$$\mathrm{d}\mathbf{X} = \mathbf{F}(\mathbf{X})\mathrm{d}t + \mathbf{G}(\mathbf{X})\mathrm{d}\mathbf{W}(t), \tag{3.21}$$

where $\mathbf{G}(\mathbf{X})$ is defined by $\mathbf{D}(\mathbf{X}) = \mathbf{G}(\mathbf{X})\mathbf{G}^T(\mathbf{X})$ and $\mathbf{W}(t)$ is composed of independent standard Brownian motions. The master equations with long-memory introduced in the previous section readily lead to the corresponding Fokker-Planck equations by the Fokker-Planck operator in Eq. (3.20).

The non-stationary master equation gives a non-autonomous Fokker-Planck equation in the form:

$$\frac{\partial}{\partial t} P(\mathbf{r},t) = \nu(t) L_{FP} P(\mathbf{r},t). \tag{3.22}$$

The corresponding sample paths, $\{\mathbf{Y}_t\}_{t\geq 0}$, are realized by

$$\mathbf{Y}_t = \mathbf{X}(R(t)), \tag{3.23a}$$

$$R(t) = \int_0^t \nu(t')\mathrm{d}t', \tag{3.23b}$$

$$\mathrm{d}\mathbf{X} = \mathbf{F}(\mathbf{X})\mathrm{d}\tau + \mathbf{G}(\mathbf{X})\mathrm{d}\mathbf{W}(\tau). \tag{3.23c}$$

In this formula, it is recognized that physical time t is associated with intrinsic time τ by a deterministic mapping $\tau = R(t)$.

The fractional master equation leads to a fractional Fokker-Planck equation in the form:

$$\frac{\partial}{\partial t}P(\mathbf{r},t) = {}_0\mathbf{D}_t^{1-\alpha} L_{FP} P(\mathbf{r},t). \tag{3.24}$$

The solution of the fractional Fokker-Planck equation is associated with that of the conventional Fokker-Planck equation having the same Fokker-Planck operator by the inverse Lévy transform in the Laplace space as

$$\hat{P}(\mathbf{r},s) = s^{\alpha-1}\hat{p}(\mathbf{r},s^{\alpha}). \tag{3.25}$$

The derivation of Eq. (3.25) is given in Appendix B. The corresponding sample paths, $\{\mathbf{Z}_t\}_{t\geq 0}$, are presented by

$$\mathbf{Z}_t = \mathbf{X}(S_t), \tag{3.26a}$$
$$S_t = \inf\{\tau; U_\alpha(\tau) > t\}, \tag{3.26b}$$
$$\mathrm{d}\mathbf{X} = \mathbf{F}(\mathbf{X})\mathrm{d}\tau + \mathbf{G}(\mathbf{X})\mathrm{d}\mathbf{W}(\tau), \tag{3.26c}$$

where $\{S_t\}_{t\geq 0}$ is a stochastic process known as a *subordinator* [38, 50] defined by $U(\cdot)$ being a strictly increasing α-stable Lévy process [51, 52]. The subordinator provides long duration, and thus can realize the effect of long-memory. The correspondence between this formula and the fractional Fokker-Planck equation is explained in Appendix C.

3.4 Summary

The GCP can describe large deviations by its stationary PDF, namely the generalized Cauchy distribution. The autocorrelation function of the GCP is analytically obtained as the exponential function with the existence of second moment.

The non-stationary master equation provides the stochastic dynamics of state transitions with long-memory by the time-scaling functions. Also, the generalized master equations present the existence of long-memory by convolution with the memory function involved in the waiting time distributions giving duration between state transitions. In the special case that the waiting time distribution has power-law property, the memory function is reduced to a power function, and then the generalized master equation leads to the fractional master equation.

The Kramers-Moyal expansion with the termination at the second term gives the corresponding Fokker-Planck equations to both master equations with realizations of sample paths.

Chapter 4

Naive statistics for one-dimensional defect turbulence

In this chapter, we present defect turbulence of the 1D CGLE with a certain parameter set by a numerical simulation. According to many previous works, we also regard the defect turbulence as many body interactions between the BN-hole and the shock like waves and then obtain three probability distributions for particle number, nearest neighbor distance, and depth of amplitude. As stochastic models for the probability distributions, we introduce a conventional master equation with its Poisson representation, a generalization of the Bayes' theorem, and a generalization of the Poisson process.

4.1 The BN-holes and the shocks in defect turbulence

In order to produce defect turbulence, we implemented a numerical simulation for the 1D CGLE with a certain parameter set $(c_1, c_2) = (1.5, -1.2)$ with system size $\Omega = 500$ being subject to periodic boundary condition. The numerical integration scheme for this work was composed of the fourth-order Runge-Kutta method for time with a step size $\Delta t = 0.01$ and the second-order central difference method for space with a resolution $\Delta x = 0.5$. Figures 4.1 show spatiotemporal dynamics of the defect turbulence in (a) amplitude and (b) phase. In the amplitude, nearest neighbor interactions between black lines and white lines, which correspond, respectively, to lower and higher values of amplitude, are recognized. In the phase, traveling sharp lines, which correspond to phase discontinuities, are recognized. Figures 4.2 show a snapshot of (a) amplitude and (b) phase at a certain time in Figs. 4.1. In the amplitude, similar profiles to the BN-holes and the shocks appear as local minimum and maximum, respectively. The value range of phase is extended in order to clarify phase discontinuities. In what follows, we call the BN-hole and the shock like waves as local depressing wave (LDW) and local standing wave (LSW), respectively. This identification is naively based on only amplitude threshold, of which in this work $|A| = 0.8$, as well as many previous works [25, 32, 53].

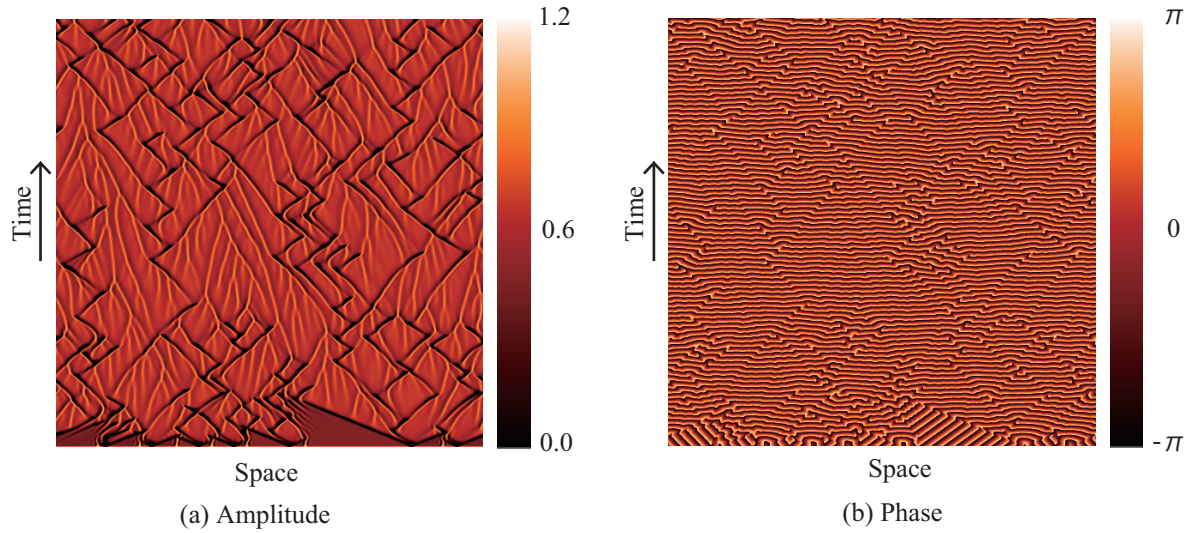

Figure 4.1: Spatiotemporal dynamics of the defect turbulence in (a) amplitude and (b) phase. The corresponding parameter set of the CGLE is $(c_1, c_2) = (1.5, -1.2)$. The system size $\Omega = 500$ being large enough to produce the defect turbulence.

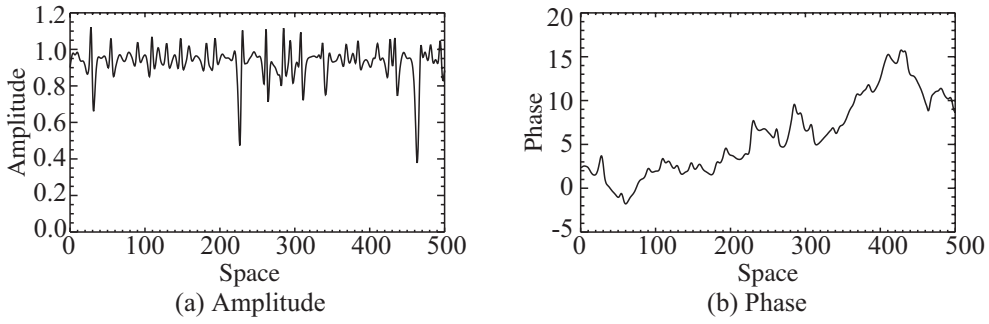

Figure 4.2: Snapshot of (a) amplitude and (b) phase at a certain time in Figs. 4.1.

4.2 Counting statistics for LDWs

We counted LDW number in the whole space at each time step and then obtained the probability distribution for them as is shown in Fig. 4.3. The probability distribution is identified well by the binomial distribution:

$$B(p,k) = {}_nC_k p^k (1-p)^{n-k}, \tag{4.1}$$

where n is the maximum LDW number in the whole space, p is the probability in generating a LDW, and k is a LDW number, respectively. The parameters in Eq. (4.1) are estimated by the moments as n = 41 and p = 0.2. In order to classify statistical property, we utlized the Fano factor, FF, defined by

$$FF = \frac{\sigma_k^2}{\langle k \rangle} \tag{4.2}$$

with $\langle k \rangle$ being the mean, and σ_k^2 being the variance. For the Poisson distribution, of which the mean and the variance are the same value, $FF = 1$. The LDW number statistics with $FF = 0.8$, being less than 1.0, is subjected to a sub-Poisson statistics, which implies the existence of LDWs bunching states by analogy of photon number statistics in quantum optics [54].

In order to elucidate the underlying mechanism of the sub-Poisson statistics, we constructed interaction scheme among LDWs and LSWs in the defect turbulence as follows: (i) two LDWs collide and then turn into one LSW, (ii) two LSWs merge into one LSW, (iii) one LDW absorbs or emits one LSW, (iv) one LDW becomes one LSW, (v) both LDW and LSW emerge from background. The integrated scheme is written down as

$$2X \xrightarrow{k_1'} Y, \tag{4.3a}$$

$$2Y \xrightarrow{k_2'} Y, \tag{4.3b}$$

$$X + Y \underset{k_4'}{\overset{k_3'}{\rightleftarrows}} X, \tag{4.3c}$$

$$X \xrightarrow{k_5'} Y, \tag{4.3d}$$

$$0 \xrightarrow{k_6'} X, \tag{4.3e}$$

$$0 \xrightarrow{k_7'} Y, \tag{4.3f}$$

where X and Y denote, respectively, LDW and LSW, and each k_i' denotes reaction constant. Although it is desirable to analyze the full scheme, we only need, here, to get the knowledge of X. For this purpose, we employed an adiabatic approximation for Y and then obtained the following reduced scheme

$$2X \xrightarrow{k_1} 0, \tag{4.4a}$$

$$0 \underset{k_3}{\overset{k_2}{\rightleftarrows}} X, \tag{4.4b}$$

with k_i being a reaction constant rate. The reduced scheme describes pair annihilation in Eq. (4.4a), emission and sinking in Eq. (4.4b), which are a key mechanism in producing sub-Poisson statistics

[55, 56], and then provides transition probabilities as

$$W(X, \Delta X, t) = k_1 X(X-1)\delta_{\Delta X,-2} + k_2 \delta_{\Delta X,1} + k_3 X \delta_{\Delta X,-1}, \tag{4.5}$$

where ΔX is transition rate of X and $\delta_{i,j}$ is the Kronecker's delta. The transition probabilities readily lead to a master equation with respect to $P(X,t)$ being the time-dependent probability distribution for X as

$$\begin{aligned}\frac{\mathrm{d}}{\mathrm{d}t}P(X,t) &= k_1(X+2)(X+1)P(X+2,t) + k_2 P(X-1,t) \\ &+k_3(X+1)P(X+1,t) - [k_1 X(X-1) + k_2 + k_3 X]P(X,t).\end{aligned} \tag{4.6}$$

In general, master equations are hard to be solved analytically. Hence, we utilized the Poisson representation of Eq. (4.6) to evaluate first and second moment. The Poisson representation, $f(\xi,t)$, for arbitrary probability distribution, $P(X,t)$, is associated with a integral transform on complex plane by

$$P(X,t) = \int_C \frac{\mathrm{e}^{-\xi}\xi^X}{X!} f(\xi,t)\mathrm{d}\xi \tag{4.7}$$

with ξ being a complex variable on an integral contour C [42]. Substituting Eq. (4.7) into Eq. (4.6), one obtains an evolution equation for $f(\xi,t)$ in the form:

$$\frac{\partial}{\partial t}f(\xi,t) = -\frac{\partial}{\partial \xi}[(-2k_1\xi^2 + k_2 + k_3\xi)f(\xi,t)] - \frac{\partial^2}{\partial \xi^2}[(k_1\xi^2)f(\xi,t)]. \tag{4.8}$$

Although the negative diffusion term in the right-hand side of Eq. (4.8) makes the forward evolution of $f(\xi,t)$ be unstable, the stationary distribution can be formally obtained as

$$f_s(\xi) = \xi^{-(2+a_2)}\exp\left(2\xi + \frac{a_1\Omega^2}{\xi}\right) \tag{4.9}$$

with $a_1 = k_2/k_1\Omega^2$ and $a_2 = k_3/k_1$. The r-th moments are evaluated on a closed loop encircling the origin of complex plane by

$$\langle \xi^r \rangle \;=\; \frac{\oint \xi^r f_s(\xi)\mathrm{d}\xi}{\oint f_s(\xi)\mathrm{d}\xi}. \tag{4.10}$$

The specific form of the moments is given by

$$\langle \xi^r \rangle = \left(\Omega\sqrt{\frac{a_1}{2}}\right)^r \frac{I_{r-(a_2+1)}(2\Omega\sqrt{2a_1})}{I_{a_2+1}(2\Omega\sqrt{2a_1})}, \tag{4.11}$$

with $I_d(\cdot)$ being the modified Bessel function [57]. With the relations that $\langle X \rangle = \langle \xi \rangle$ and $\sigma_X^2 = \langle \xi^2 \rangle - \langle \xi \rangle^2 + \langle \xi \rangle$, the FF is asymptotically evaluated by

$$FF = \frac{3}{4}\frac{\Omega\sqrt{a_1/2} + O(1)}{\Omega\sqrt{a_1/2} + O(1)} \approx \frac{3}{4}. \tag{4.12}$$

This value gives a good approximation for our simulation result. Thus the reduced interaction scheme can be essential to produce the sub-Poisson nature in the counting statistics for LDW.

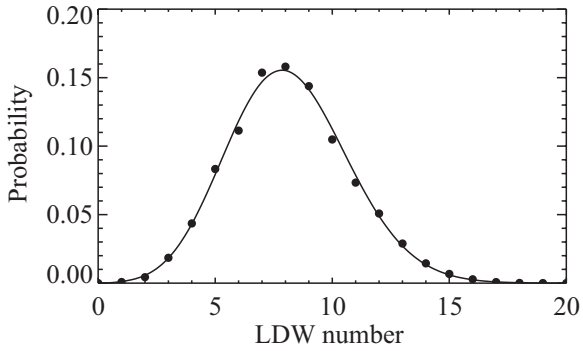

Figure 4.3: The probability distribution for LDW number are denoted by the black circles, being compared with the binomial distribution as the solid line.

4.3 Inter-LDWs distance statistics

Inter-LDWs distance relates to nearest neighbor interaction between LDWs. The information about it takes the range where local interactions between LDWs occur frequently. Figure 4.4 shows that the probability distribution for inter-LDWs distance has two different characteristics. One is a sharp peak around 5.5, the other is an asymmetry hill shape. The former peak seems to be originated from the LDWs bunching states as was mentioned above. Without this peak, the probability distribution is identified by the hyper gamma distribution in the form:

$$f_{HG}(y;\alpha,\beta,\gamma) = \frac{\beta^{\gamma/\alpha}}{\Gamma(\gamma/\alpha)} y^{\gamma-1}\exp(-\beta y^{\alpha}), \tag{4.13}$$

where y is a random variable, α, β, γ are real parameters, and $\Gamma(\cdot)$ is the gamma function. Figure 4.5 shows the hill-type shape and the hyper gamma distribution with the parameters $\alpha = 1.18$, $\beta = 24.2$ and $\gamma = 1.79$. Here, the horizontal axis in this figure is rescaled. The tail of the hyper gamma distribution has an exponential decay, which validate the local interactions between the LDWs.

Among many possible physical explanations giving rise to the hyper gamma distribution, we adopted the method of superstatistics [58]. Assumed that the LDWs are subjected to a Poisson configuration, the probability distribution for inter-LDWs distance is described by an exponential distribution. In the context of superstatistics, the parameter of the exponential distribution is also a random variable. Hence, the hyper gamma distribution can be described by

$$f_{HG}(y;\alpha,\beta,\gamma) = \int_0^{\infty} \lambda\exp(-\lambda y) g(\lambda)\mathrm{d}\lambda \tag{4.14}$$

with $g(\lambda)$ being a PDF of λ, which is governed by

$$D_\lambda \left[D_\lambda^{\alpha} - \frac{1}{\alpha\beta} D_\lambda \lambda + \frac{2-\gamma}{\alpha\beta} \right] g(\lambda) = 0, \tag{4.15}$$

where D_λ denotes the operator defined by

$$D_\lambda = \frac{\mathrm{d}}{\mathrm{d}\lambda} + \frac{1}{\lambda}. \tag{4.16}$$

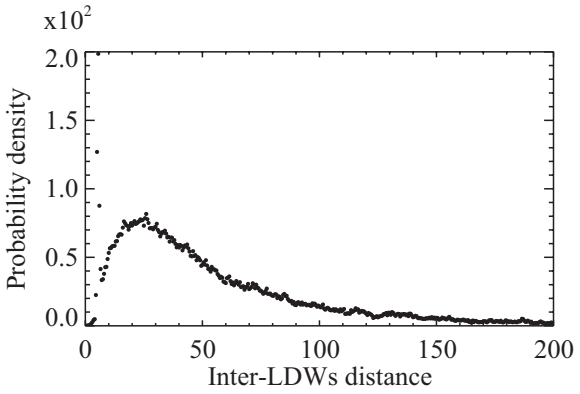

Figure 4.4: The probability distribution for inter-LDW distance. There are two different characteristics that the sharp peak around 5.5 and the asymmetry hill shape.

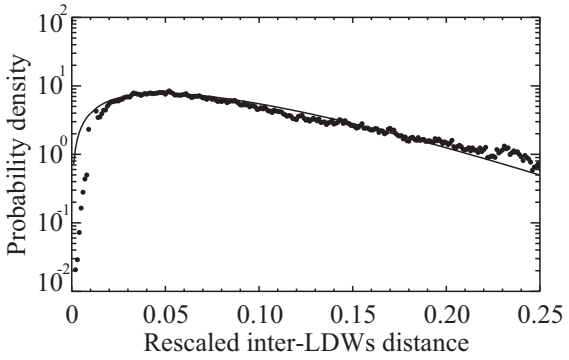

Figure 4.5: A part of the probability distribution without the sharp peak. Black circles are collected data. Solid line is the hyper gamma distribution with the parameters $\alpha = 1.18$, $\beta = 24.2$ and $\gamma = 1.79$.

Although the specific form of $g(\lambda)$ can be obtained from Eq. (4.15), the α-th order operator D_{λ}^{α}, since α is not integer value in our case, makes Eq. (4.15) difficult to solve analytically. However, in special case that $\alpha = 1$, Eq. (4.15) leads to the hypergeometric differential equation, and thus $g(\lambda)$ is analytically obtained in terms of the hypergeometric function giving the gamma distribution.

4.4 LDW depth statistics

LDW depth from background is a kind of rare events characterized by occurrence of bursts, which also takes the help for understanding the physical nature. In order to carry out statistical analysis, we collected LDW depths in the whole space at each time and then dealt with them as a time series. The depth is defined a length from the background, $|A| = 0.8$, to the bottom, $|A| = 0$. Thereby the maximum value of LDW depth is 0.8 in this case. Figure 4.6 shows the probability distribution for rescaled LDW depth. The truncation of the probability distribution is due to the definition of LDW

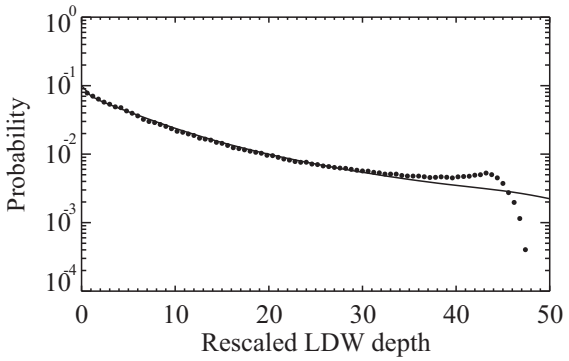

Figure 4.6: The probability distribution for LDW depth. Black circles are collected data from our simulation, which are characterized by a pawer law tail and truncation. The definition of the LDW depth causes the truncation. Solid line is the probability distribution given by the STFPP.

depth.

Assuming that the LDWs bunching states cause strong spatial correlations, we employed a space-time fractional Poisson process (STFPP) [59], which can describe coherence in time and space, as a model for LDW depth statistics. The STFPP is described by a backward operator B with a power exponents $\mu, \nu \in (0, 1)$ in the form:

$$\frac{\mathrm{d}^\nu}{\mathrm{d}z^\nu} p(l, z) = -\theta^\mu (1 - B)^\mu p(l, z), \tag{4.17}$$

with θ being a real parameter. The solution of Eq. (4.17) is given by

$$p(l, z) = \frac{(-1)^l}{l!} \sum_{r=0}^{\infty} \frac{(-\theta^\mu z^\nu)^r}{\Gamma(\nu r + 1)} \frac{\Gamma(\mu r + 1)}{\Gamma(\mu r + 1 - l)}. \tag{4.18}$$

The probability distribution in Eq. (4.18) with the parameters $\mu = 0.605$, $\nu = 0.72$, and $\lambda = 0.05$ is compared with the collected data from our simulation in Fig. 4.6. The theoretical probability distribution gives a good agreement with the power law tail in that of the simulation data. This result indicates that there are strong spatial and temporal correlations in the defect turbulence.

4.5 Summary

Regarding the defect turbulence as the birth-death process of LDWs and LSWs, we carried out statistical analysis for LDW number, inter-LDWs distance, and LDW depth. The counting statistics for LDW number was subjected to a sub-Poisson statistics, which implies the existence of LDWs bunching states. This nature was explained by the master equation derived from the interaction scheme of LDWs and LSWs with its Poisson representation. In the probability distribution for inter-LDWs distance, a sharp peak and an asymmetric hill shape were recognized. The peak seemed to be caused by the LDWs bunching states. The hill shape was identified by the hyper gamma distribution with superstatistics for a Poisson configuration. The statistics for LDW depth was modeled by a

space time fractional Poisson process, which can describes the effect of strong correlations in space and time.

Chapter 5

Birth-death process of local structures in defect turbulence

In the previous chapter, we regarded naively the defect turbulence as a birth-death process of LDWs and LSWs, which are identified by only amplitude value. However, the concept of the coherent structures explained in chapter 2 suggests that localized waves of the 1D CGLE should be discriminated by both amplitude and phase. Here, we identify stochastic dynamics of local structures with the use of both amplitude and phase in the defect turbulence.

5.1 Local structures in defect turbulence

In the concept of the coherent structures, localized nonlinear waves of the 1D CGLE are classified based on information about both amplitude and phase. This classification is plausible because the CGLE describes evolution of a complex variable filed composed of amplitude and phase. Indeed, the concept of the coherent structures has been introduced to spatiotemporal disorder of the 1D CGLE as "local structures", which are defect, hole, and MAW, and then, their identification methods have been developed [60].

A defect is characterized by a nonzero winding number, and thus we can capture defects as phase singular points in the x–t plane by the criterion $\frac{1}{2\pi}\oint \nabla\varphi\cdot\mathrm{d}\mathbf{r}\neq 0$, where $\varphi = \arg(A)$. The contour integrals have been numerically evaluated on each discrete lattice (i, j), being discretized as $i = x/\Delta x$ for space and $j = t/\Delta t$ for time, in terms of the phase on site, $\varphi_{i,j}$. A defect is captured if and only if its phase discontinuity vanishes on the integral contour: $\varphi_{i-1,j-1} \rightarrow \varphi_{i+1,j-1} \rightarrow \varphi_{i+1,j+1} \rightarrow \varphi_{i-1,j+1} \rightarrow \varphi_{i-1,j-1}$ (see Fig. 5.1(a)). Lifetimes of defects are thereby less than the discretized time interval Δt.

A hole is defined as a local minimum of amplitude with a phase jump (see Fig. 5.1(b)). Although defects, for which the winding numbers are not zero, also satisfy this condition, the winding numbers of holes are zero. In other words, phase jumps of holes pass through their integral contours without vanishing. Hence we can distinguish holes from defects.

As mentioned above, an MAW appears as the stable branch of a saddle node bifurcation whereas a hole appears as the unstable one in the context of coherent structures. It is thus difficult to distinguish MAWs from holes in the defect turbulence, where both the stable and the unstable branches coexist.

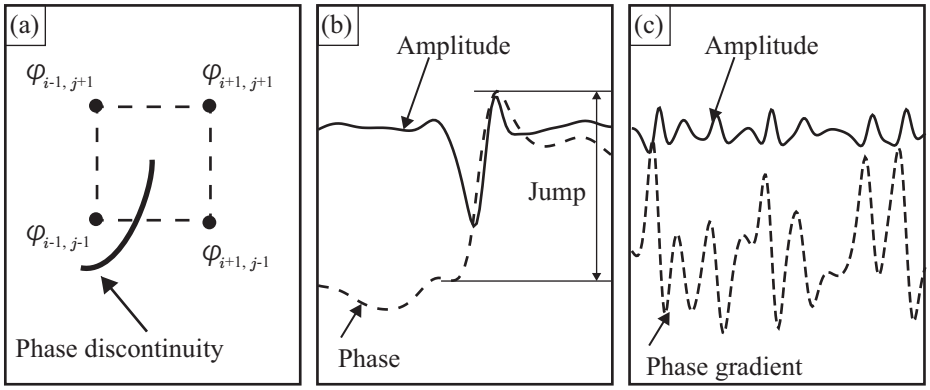

Figure 5.1: Conceptual diagram of the definition of the local structures. (a) Defects are identified by phase singularities at which the winding numbers in the discretized x–t plane are not zero. A defect is thus captured if and only if a phase discontinuity vanishes on the discretized integral contour: $\varphi_{i-1,j-1}\rightarrow\varphi_{i+1,j-1}\rightarrow\varphi_{i+1,j+1}\rightarrow\varphi_{i-1,j+1}\rightarrow\varphi_{i-1,j-1}$. (b) Holes are identified by local minima of the amplitude at phase jumps. Holes can thereby be captured after defect identification because defects also have the same characteristic. (c) MAWs are identified by local maxima of the amplitude with steep phase gradients exceeding a specific value.

An MAW is defined by a local maximum of amplitude with a steep phase gradient exceeding a specific value (see Fig. 5.1(c)). To avoid confusing MAWs with holes in the defect turbulence, we have performed the procedure for MAWs after defects and holes had been identified completely.

5.2 Counting statistics for local structures

After identifying the local structures, we investigated their counting statistics. Figure 5.2 shows the probability distributions for the number of (a) defects, (b) holes, and (c) MAWs. The specific values of the FF are (a) 1.00 for defects, (b) 1.01 for holes, and (c) 1.04 for MAWs. Thus, all these probability distributions are identified by the Poisson distribution

$$P(n) = \frac{\lambda^n}{n!}\mathrm{e}^{-\lambda}, \tag{5.1}$$

where n is the number of each local structure and λ is the constant parameter estimated as the average value of n.

In the previous section, we showed that LDW number is subjected to the sub-Poisson statistics, which implies the existence of LDWs bunching states with the evidences that are the pair annihilation of LDWs and the sharp peak in the probability distribution for inter-LDWs distance (Fig. 5.3(b)). As is shown in Fig. 5.3(a), the sharp peak is caused by nearby amplitude dips of holes and MAWs. The sharp peak is automatically eliminated from the probability distribution for inter-holes distance by the identification of the local structures (Fig. 5.3(c)). Thus, the sub-Poisson nature in LDW number statistics can be regarded as an unexpected illusion caused by an unsuitable identification method based on only amplitude value.

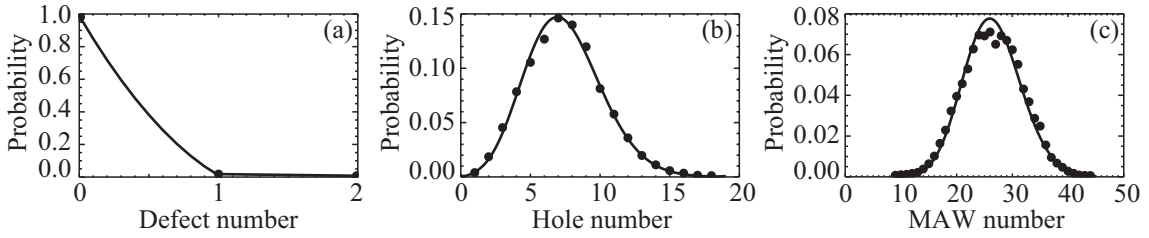

Figure 5.2: Probability distributions for the number of (a) defects, (b) holes, and (c) MAWs. The number of each local structure is counted in the whole space at each time step of the numerical simulation. The black circles indicate the collected data from the numerical simulation and the solid lines present the Poisson distributions with estimated parameters of (a) $\lambda = 0.0105$, (b) $\lambda = 7.43$, and (c) $\lambda = 26.5$.

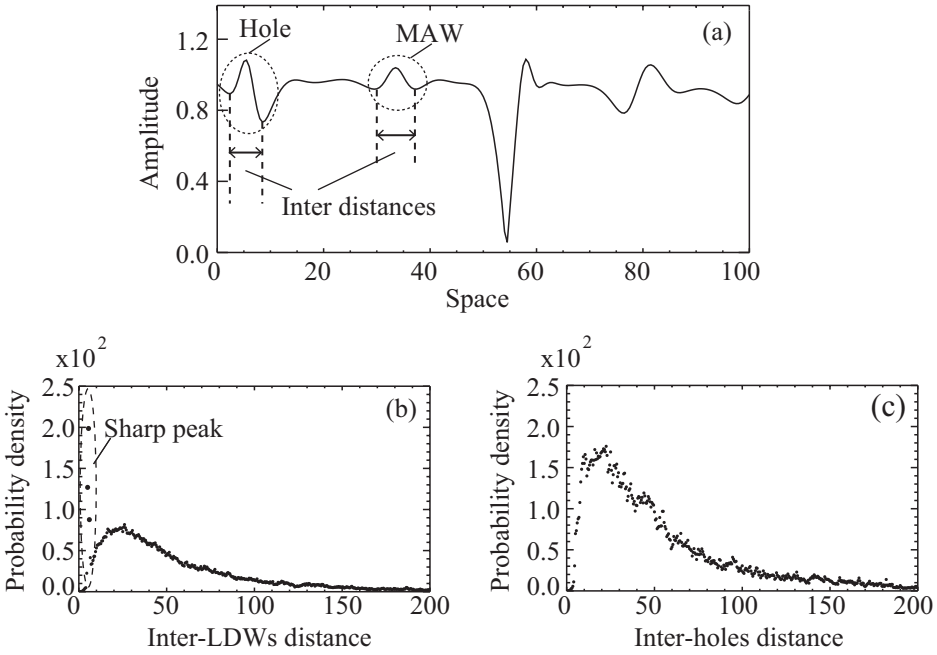

Figure 5.3: (a) Distances between nearby amplitude dips, regarded as inter-LDWs distances in the previous chapter. However, the amplitude dips are in fact parts of either holes or MAWs. The probability distributions for (b) inter-LDWs distance and (c) inter-holes distance. The sharp peak in (b) is automatically eliminated from (c), which means that the identification method based on only the amplitude causes confusion with regard to the sub-Poisson statistics.

The interaction scheme of the local structures has been investigated to understand the dynamical properties of systems with disorder. A hole can transform into a defect when the amplitude dip of the hole reaches zero, followed by the defect generating another hole and transforming back to a hole [61]. Holes and MAWs transform into each other through saddle-node bifurcations [60]. MAWs emerge from and sink into the background; moreover, splitting and merging processes of MAWs are dominant in turbulent regimes [62]. The interaction scheme observed can be written as

$$H \underset{k_2}{\overset{k_1}{\rightleftarrows}} D, \tag{5.2a}$$

$$D \xrightarrow{k_3} D + H, \tag{5.2b}$$

$$H \underset{k_5}{\overset{k_4}{\rightleftarrows}} M \tag{5.2c}$$

$$0 \underset{k_7}{\overset{k_6}{\rightleftarrows}} M, \tag{5.2d}$$

$$M \underset{k_9}{\overset{k_8}{\rightleftarrows}} 2M, \tag{5.2e}$$

where D, H, M, and k_i denote a defect, a hole, an MAW, and their reaction rates, respectively. Note that there are not the pair annihilation as observed in the birth-death process of the LDWs and LSWs because the process is a misunderstanding of the interaction between a hole and an MAW, which is caused by the unsuitable identification methods. The corresponding conventional master equation is derived from the above scheme as

$$\begin{aligned}\frac{\mathrm{d}}{\mathrm{d}t}P(d,h,m;t) = {} & k_1(d+1)P(d+1,h-1,m;t) + k_2(h+1)P(d-1,h+1,m;t) \\ & + k_3 dP(d,h-1,m;t) + k_4(h+1)P(d,h+1,m-1;t) \\ & + k_5(m+1)P(d,h-1,m+1;t) + k_6\Omega P(d,h,m-1;t) \\ & + k_7(m+1)P(d,h,m+1;t) + k_8(m-1)P(d,h,m-1;t) \\ & + k_9\Omega^{-1}(m+1)mP(d,h,m+1;t) \\ & - [k_1 d + k_2 h + k_3 d + k_4 h + k_5 m + k_6\Omega \\ & + k_7 m + k_8 m + k_9\Omega^{-1}m(m-1)]P(d,h,m;t),\end{aligned} \tag{5.3}$$

where d, h, and m denote the number of defects, holes, and MAWs, and Ω is the system size. In general, a multivariable Poisson distribution is derived from the master equations for stationary states under the independence condition [42]. Thus, assuming that $P(d,h,m;t) = P_0(d,h,m;t) + \epsilon P_1(d,h,m;t)$ with $P_0(d,h,m;t) = \xi(d;t)\eta(h;t)\zeta(m;t)$ and ϵ decaying more rapidly than Ω^{-1} with $\Omega\to\infty$, we can obtain the evolution equations of the marginal PDFs, $\xi(d;t)$, $\eta(h;t)$, and

$\zeta(m;t)$ from Eq. (5.3) as

$$\frac{\mathrm{d}}{\mathrm{d}t}\xi(d;t) = k_1(d+1)\xi(d+1;t) + k_2\langle h\rangle_\eta \xi(d-1;t) - [k_1 d + k_2\langle h\rangle_\eta]\xi(d;t), \tag{5.4a}$$

$$\frac{\mathrm{d}}{\mathrm{d}t}\eta(h;t) = (k_2+k_4)(h+1)\eta(h+1;t) + (k_1+k_3)\langle d\rangle_\xi \eta(h-1;t) - [(k_2+k_4)h + (k_1+k_3)\langle d\rangle_\xi]\eta(h;t), \tag{5.4b}$$

$$\frac{\mathrm{d}}{\mathrm{d}t}\zeta(m;t) = (k_9\Omega^{-1}m + k_5 + k_7)(m+1)\zeta(m+1;t) + [k_4\langle h\rangle_\eta + k_8(m-1) + k_6\Omega]\zeta(m-1;t) - [k_9\Omega^{-1}(m-1) + k_5 + k_7]m\zeta(m;t) - [k_4\langle h\rangle_\eta + k_8 m + k_6\Omega]\zeta(m;t), \tag{5.4c}$$

where $\langle d\rangle_\xi$ and $\langle h\rangle_\eta$ are the mean values of ξ and η with respect to $\xi(d;t)$ and $\eta(h;t)$, respectively. Since the PDFs for the number of each local structure were evaluated in the stationary state, the stationary PDFs, $\xi_s(d)$, $\eta_s(h)$, and $\zeta_s(m)$, in a large system where $\epsilon\to 0$, are readily obtained from Eqs. (5.4) as the Poisson distributions:

$$\xi_s(d) = \frac{\lambda_\xi^d}{d!}\mathrm{e}^{-\lambda_\xi}, \quad \lambda_\xi = \frac{k_2\langle h\rangle_\eta}{k_1}, \tag{5.5a}$$

$$\eta_s(h) = \frac{\lambda_\eta^h}{h!}\mathrm{e}^{-\lambda_\eta}, \quad \lambda_\eta = \frac{(k_1+k_3)\langle d\rangle_\xi}{k_2+k_4}, \tag{5.5b}$$

$$\zeta_s(m) = \frac{\lambda_\zeta^m}{m!}\mathrm{e}^{-\lambda_\zeta}, \quad \lambda_\zeta = \frac{k_6\Omega}{k_5+k_7}. \tag{5.5c}$$

The conventional master equations in Eqs. (5.4) can be written in the form:

$$\frac{\mathrm{d}}{\mathrm{d}t}P(n;t) = J(n+1;t) - J(n;t), \tag{5.6}$$

where $J(n;t)$ is a functional of $P(n;t)$, the stochastic flux [42]. In the stationary state, $J_s(n) = 0$ leads to the recursion relation

$$P(n) = \frac{c(n-1)}{a(n)}P(n-1) \tag{5.7}$$

with $a(n)$ and $c(n)$, respectively, being an annihilation and a creation rate. The ratio, $c(n-1)/a(n)$, must be proportional to n^{-1} for stationary Poisson processes. Figure 5.4 shows the creation and the annihilation rates of the local structures estimated by using the least-square method. The creation rates (Fig. 5.4(a), (c), and (e)) are estimated as constant values, $c(n) = c_0$, and the annihilation rates (Fig. 5.4(b), (d), and (f)) are proportional to n, $a(n) = a_1 n$. The values of the creation and the annihilation rates for smaller numbers of MAWs less than 21 were also counted. In estimating the creation and the annihilation rates of MAWs, we have utilized the data for the values of them for the numbers for $21 \leq n \leq 45$, since the error bar increases for smaller values of n in c_0, and for larger values of n in a_1. Hence, the values c_0, a_1 for $21 \leq n \leq 45$ are depicted in Figs. 5.4(e), (f). This result gives a plausible explanation for the appearance of Poisson statistics in the stationary state.

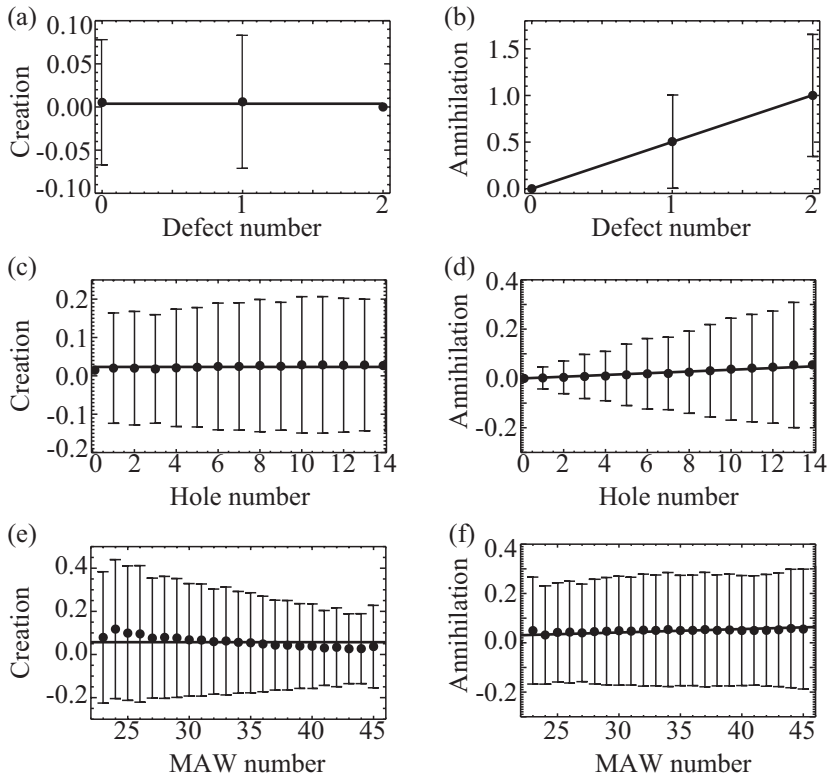

Figure 5.4: Creation rates of (a) defects, (c) holes, and (e) MAWs, and annihilation rates of (b) defects, (d) holes, and (f) MAWs. These creation and annihilation rates were estimated by using the least-squares method. In each figure, the black circles indicate the mean values with the vertical bars indicating the standard deviations obtained from the numerical simulation. The values of each creation and annihilation rate, (c_0, a_1), are (0.00376, 0.501) for defects, (0.0232, 0.0037) for holes, and (0.057, 0.00147) for MAWs.

5.3 Interarrival time statistics for local structures

The statistical properties of interarrival times of defects, lifetimes of holes, and that of MAWs give us information on the time code for the birth-death process of the local structures, while the counting statistics provide information on the rate code. These two codes provide complementary information. In order to obtain the PDFs for interarrival times of defects, lifetimes of holes, and that of MAWs, we have to know the time evolution of the PDFs for the number of the local structures. The conventional master equation of each local structure in the large system is

$$\frac{\mathrm{d}}{\mathrm{d}t}P(n;t) = c_0[P(n-1;t) - P(n;t)] + a_1[(n+1)P(n+1;t) - nP(n;t)]. \tag{5.8}$$

The exact solution is given by

$$P(n;t) = \frac{1}{n!}\left[\frac{c_0}{a_1}(1-\mathrm{e}^{-a_1 t})\right]^n \exp\left[-\frac{c_0}{a_1}(1-\mathrm{e}^{-a_1 t})\right]. \tag{5.9}$$

The corresponding PDFs for the interarrival times of defects, and the lifetimes of holes and MAWs, $f_M(t)$, are readily obtained from the relation $f_M(t) = -\frac{\mathrm{d}}{\mathrm{d}t}P(0;t)$ as

$$f_M(t) = c_0 \mathrm{e}^{-a_1 t} \exp\left[-\frac{c_0}{a_1}(1-\mathrm{e}^{-a_1 t})\right]. \tag{5.10}$$

Figure 5.5 shows the probability distributions for them obtained from the numerical simulation; these probability distributions are characterized by fat tails and specific peaks. In contrast, the theoretical PDF, $f_M(t)$, in Eq. (5.10) shows a double-exponential decay.

In the amplitude dynamics of the defect turbulence, one can see zigzag motions of traveling holes with oscillating amplitudes. Figures 5.6 (a) and (b) show a zigzag motion of a traveling hole and a defect generation caused by the traveling hole moving from the right side to the left side, respectively. In Fig. 5.6 (a), the white circles on the edges of the zigzag black line correspond to defects generated from the traveling hole. In Fig. 5.6 (b), the hole moving from the right side changes to a defect, which generates another hole moving to the left side when the amplitude of the traveling hole reaches zero. The defect then changes into a hole moving to the right side. Hence the intervals between nearest neighbor defects in the direction of time in Fig. 5.6 (a) correspond to both the interarrival times of defects and the lifetimes of holes. In other words, a kind of periodicity involved in the zigzag motions of holes causes the specific peaks in Figs. 5.5 (a) and (b).

We assume that the zigzag motions of holes enhance the creation rates of defects and holes as a superposition of Lorentzian-type functions involved in periods of the zigzag motions. In addition, a time-scaling function is introduced to realize the effects of long-memory. There are two ways to take into account the effect of long-memory for master equations: 1. generalized master equations with convolution-type memory functions involved in waiting-time PDFs of reactions, and 2. non-stationary, convolutionless-type master equations with time-dependent reaction rates. Here, we

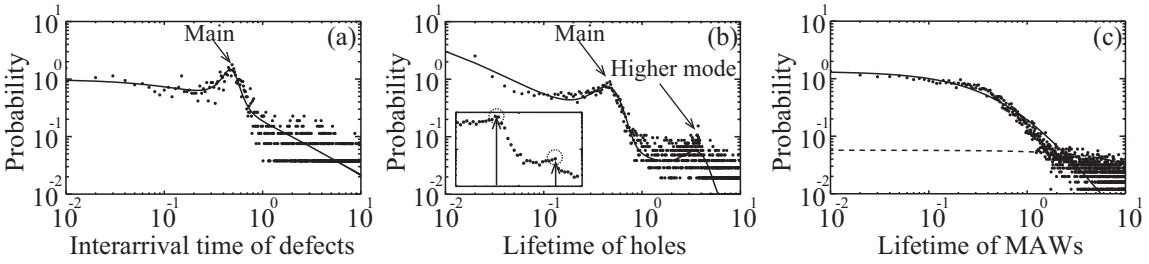

Figure 5.5: Probability distributions for (a) the interarrival times of defects τ_D, the lifetimes (b) of holes l_H, and (c) that of MAWs l_M. The window in (b), where one can see the main and higher mode peaks, is an enlarged view of averaged data. In each figure, the black circles present the numerically obtained probability distribution and the solid line is the theoretical PDF of the non-Markovian model $f_{nM}(\cdot)$ in Eq. (5.13). The dashed line in (c) is the theoretical PDF of the Markovian model $f_M(l_M)$ in Eq. (5.10). The parameters of the theoretical PDFs are estimated by using the least-square method as follows: (a) $(c_0, a_1, \kappa_{00}, \kappa_{10}, T_0, \alpha_0, \nu_0, \nu_1) = (3.76\times10^{-3}, 0.501, 3.72, 59.5, 0.48, 1.53, 3.7\times10^{-4}, 4.23)$, (b) $(c_0, a_1, \kappa_{00}, \kappa_{10}, T_0, \alpha_0, \kappa_{01}, \kappa_{11}, T_1, \alpha_1, \nu_0, \nu_1) = (2.32\times10^{-2}, 3.7\times10^{-3}, 7.0, 6.65, 0.48, 4.43, 3.74, 7.16\times10^{-2}, 3.76, 7.65, 3.02\times10^{-2}, 164.0)$, and (c) $(c_0, a_1, \nu_0, \nu_1) = (5.7\times10^{-2}, 1.47\times10^{-3}, 30.1, 1.28)$.

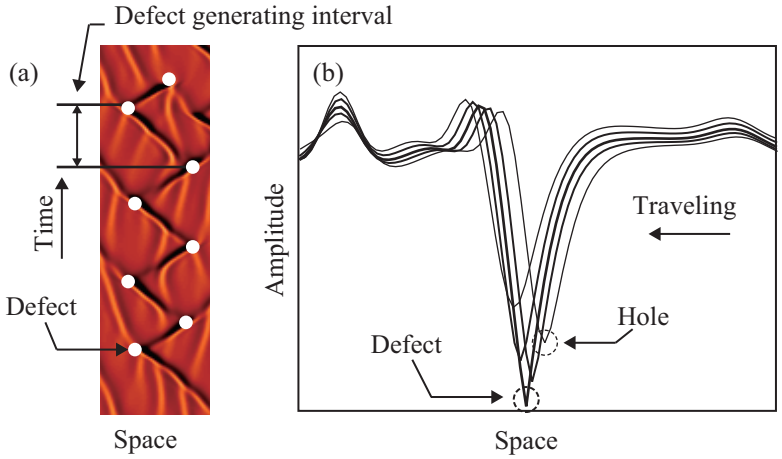

Figure 5.6: (a) Zigzag motion of a traveling hole extracted from Fig. 4.1(a). The black line is a trajectory of the traveling hole and the white circles are defects. The intervals between nearest neighbor defects in the direction of time correspond to both the interarrival times of defects and the lifetimes of the holes. (b) Defect generation caused by the traveling hole moving from the right side to the left side. The defect is generated when the amplitude of the traveling hole reaches zero.

adopt the latter-type non-Markovian master equation in the form:

$$\frac{\mathrm{d}}{\mathrm{d}t}P(n;t) = c_0(1+\psi(t))\nu(t)[P(n-1;t) - P(n;t)] + a_1\nu(t)[(n+1)P(n+1;t) - nP(n;t)], \tag{5.11a}$$

$$\psi(t) = \sum_j \frac{\kappa_{0j}}{[1+\kappa_{1j}(t-T_j)^2]^{\alpha_j}}, \tag{5.11b}$$

$$\nu(t) = \frac{\nu_0}{1+\nu_1 t}, \tag{5.11c}$$

where $\psi(t)$ is the superposition of the Lorentzian-type functions including sets of real parameters $\{(\kappa_{0j}, \kappa_{1j}, T_j, \alpha_j)\}_j$, and $\nu(t)$ is a monotonically increasing positive function with two real parameters (ν_0, ν_1). The time evolution of the PDF is exactly given by

$$P(n;t) = \frac{[\Phi(t)]^n}{n!}\exp[-\Phi(t)], \tag{5.12a}$$

$$\Phi(t) = \frac{c_0}{a_1}\left[1 - \frac{1}{(1+\nu_1 t)^{\frac{a_1\nu_0}{\nu_1}}}\right] + \frac{c_0\theta(t)}{(1+\nu_1 t)^{\frac{a_1\nu_0}{\nu_1}}}, \tag{5.12b}$$

$$\theta(t) = \int_0^t \nu_0(1+\nu_1 t')^{\frac{a_1\nu_0}{\nu_1}-1}\psi(t')\mathrm{d}t'. \tag{5.12c}$$

The derivations of these formula is given in Appendix D. The corresponding PDFs of the interarrival times of defects, the lifetimes of holes, and that of MAWs are readily obtained as

$$f_{nM}(t) = -\frac{\mathrm{d}\Phi(t)}{\mathrm{d}t}\exp[-\Phi(t)]. \tag{5.13}$$

Since $\Phi(t)$ satisfies $\lim_{t\to\infty}\Phi(t) = c_0/a_1$, $P(n;t)$ leads to the Poisson distribution at stationary state, which is consistent with the result of the counting statistics as previously mentioned. In a special case, $\psi(t) = 0$ for MAWs, $f_{nM}(t)$ is simplified as

$$f_{nM}(t) = \frac{c_0\nu_0}{\nu_1}(1+\nu_1 t)^{-\frac{a_1\nu_0}{\nu_1}-1}\exp\left[-\frac{c_0}{a_1}\left(1-(1+\nu_1 t)^{-\frac{a_1\nu_0}{\nu_1}}\right)\right]. \tag{5.14}$$

The theoretical PDFs for the interarrival times of defects, the lifetimes of holes, and that of MAWs, $f_{nM}(t)$, are compared with those of the numerical results in Fig. 5.5. For the interarrival times of defects, τ_D, $f_{nM}(\tau_D)$ captures the "power-law" behaviors for both low and high values of τ_D and the specific peaks involved in a period of the zigzag motions. The non-Markovian theoretical PDF $f_{nM}(l_H)$, for the lifetimes of holes, l_H, include a higher mode at $T_1 = 3.76$ in addition to the main peak at $T_0 = 0.48$, which may be generated from the nonlinearity of the system. The Markovian description, $f_M(l_M)$, and the non-Markovian one, $f_{nM}(l_M)$, are compared for the lifetimes of MAWs. The non-Markovian PDF $f_{nM}(l_M)$ agrees quite well with the numerical result because of the effect of the time-scaling function describing the "power-law" relaxations for both low and high values of l_M. However, the double-exponential decay, which is characteristic of the Markovian PDF $f_M(l_M)$, cannot capture the "power-law" relaxations. From these observations, we conclude that our non-Markovian model can describe the effects of both the zigzag motions and the long-memory in the birth-death process.

5.4 Summary

In this chapter, we investigated the defect turbulence via the birth-death process of the local structures. After identifying defects, holes, and MAWs, we performed an appropriate statistical analysis for the number fluctuations, the interarrival times of defects, the lifetimes of holes, and that of MAWs. All the PDFs of the number of each local structure are subjected to the Poisson statistics, which is consistent with the analytical result derived from the master equation based on the interaction scheme of the local structures. In addition, we shed light on the existence of long-memory and specific time scales in the interarrival times of defects, the lifetimes of holes, and that of MAWs, and have elucidated that their characteristics—"power laws" and specific peaks in the PDFs—can be identified by the non-Markovian master equation with time-dependent reaction rates. The non-Markovian master equation is characterized by the slowly varying time scale function and the superposition of the Lorentzian type functions, which reflect the power-laws and the specific time peaks in the PDFs, respectively. These characteristics imply that the rather deterministic processes of the local structures, such as traveling holes and MAWs with long lifetimes and zigzag motions of holes, remain in the defect turbulence. In other words, the defect turbulence is not fully random spatiotemporal dynamics.

Chapter 6

Hole velocity fluctuation

In this chapter, we discuss the kinetics of the holes in the defect turbulence. Each hole can be traced by the identification method introduced in the previous chapter. If each hole velocity varies under different rules, hole velocities in the whole system are expected to be subjected to a probability distribution. Then, we try to provide a stochastic model with the hole velocity fluctuation.

6.1 Hole velocity in defect turbulence

In the context of the coherent structures, velocity of them has to be constant. Likewise the homoclinic holes, velocity of a hole in the defect turbulence is thus expected to be constant. In order to estimate velocity of each hole, we traced and labeled each hole in the defect turbulence by the identification method introduced in the previous chapter. Then, we calculated hole velocities by slopes of paths of the holes at each time.

Figures 6.1 shows three representative paths of the holes with their velocity diagrams. One can see three different motions in these figures. A straight line in Fig. 6.1(a) is expected to have a constant velocity. Indeed, the corresponding velocity diagram in Fig. 6.1(b) shows a nearly constant velocity. This is an evidence that the coherent structures like localized wave, which travels with a constant velocity, exists in the defect turbulence. However, the local structures with the different properties, namely non-constant velocities, are observed. In Fig. 6.1(c), a relatively gentle curve is recognized, which indicates the existence of deceleration in the corresponding velocity diagram as is shown in Fig. 6.1(d). Figure 6.1(e) shows a strange shape with a velocity diagram having a local minima in Fig. 6.1(f). Here one can see both acceleration and deceleration in the motion of the hole.

It is considered that there are two ways in modeling the kinetics of the hole velocity. One is a deterministic motion, the other is a stochastic process. Modeling a deterministic motion for each hole is a hard work since the holes exhibit different motions. Thus, we try to construct a stochastic model which describe hole velocity fluctuations in the whole space without discriminating between the holes in the next section.

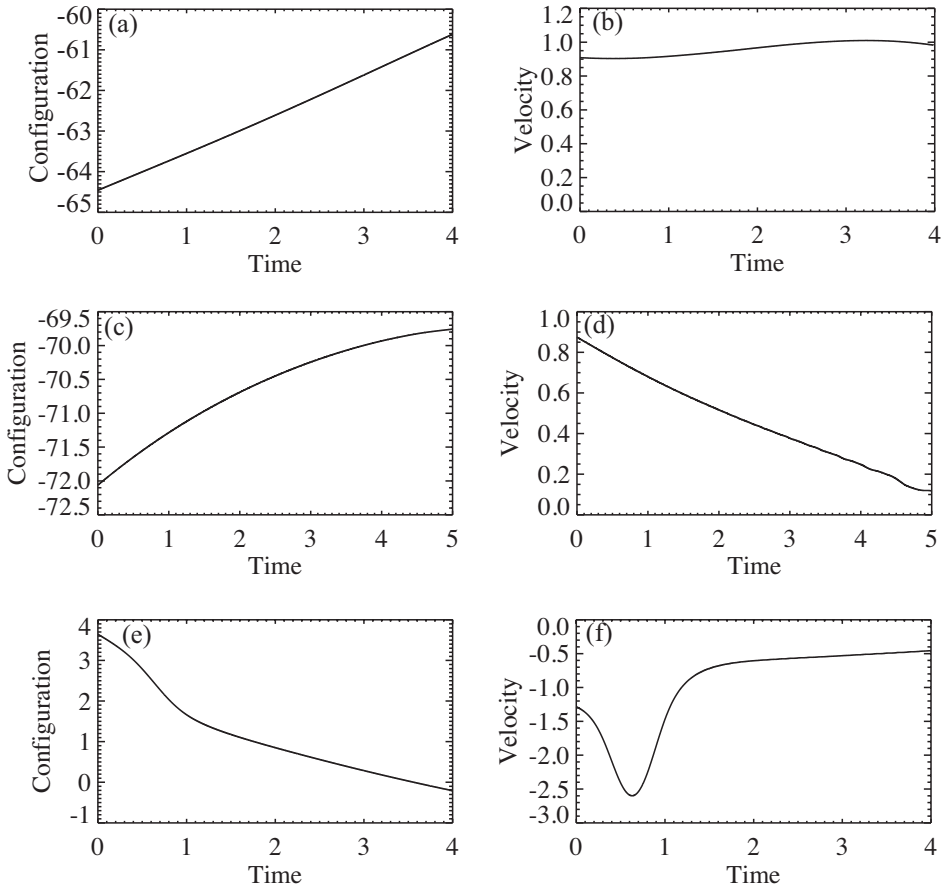

Figure 6.1: Three representative paths of holes with the corresponding velocity diagrams. The left figures are paths of holes, and the right figures are the corresponding velocity diagrams.

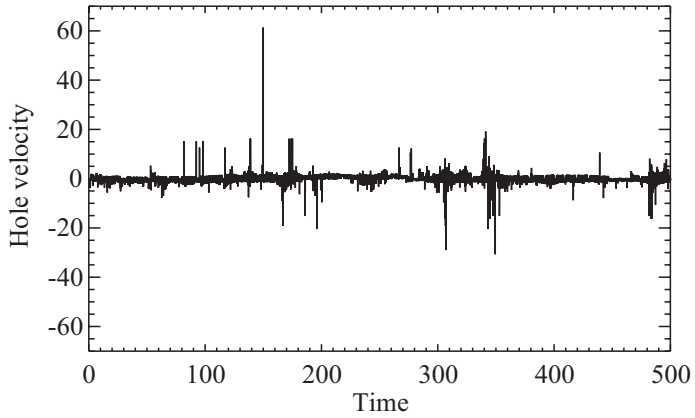

Figure 6.2: Time history of hole velocity fluctuation. Each hole velocity in this graph is collected at position x in the space at each time.

6.2 Stochastic process for hole velocity fluctuations

Without discrimination, we collected the hole velocities at position x in the space at each time, and then regarded this data set as a time series of hole velocity fluctuations. Figure 6.2 shows a time history of hole velocity fluctuation. One can see burst events in the velocity fluctuation, which can produce large deviations. Indeed, the bursts in the time series give fat tails in the probability distribution for hole velocity fluctuation denoted by black circles in Fig. 6.3, which was obtained with the help of the Rozenblatt-Parzen kernel density estimator [38]. The collected probability distribution is identified by the generalized Cauchy distribution,

$$P_s(v) = \frac{a^{2b-1}}{B(b-1/2,1/2)} \frac{1}{(v^2+a^2)^b}, \tag{6.1}$$

denoted by the solid line in Fig. 6.3. The parameters in Eq. (6.1) were estimated by the maximum likelihood method as $a = 0.426$ and $b = 1.67$. In addition, the autocorrelation coefficients of the hole velocity fluctuation was obtained from the time series. The autocorrelation coefficients have power-law property as is denoted by black circles in Fig. 6.4, which suggests that the hole velocity fluctuation has to be modeled by a class of generalized Cauchy processes with long-memory. For this purpose, two candidates are considered in what follows.

One candidate is a non-autonomous generalized Cauchy process (NAGCP) in the form:

$$V_t^{na} = X(R(t)), \tag{6.2a}$$

$$R(t) = \int_0^t \nu(t')\mathrm{d}t', \tag{6.2b}$$

$$\mathrm{d}X(t) = -\gamma X(t)\mathrm{d}t + \sqrt{2D_m}X(t)\mathrm{d}W_m(t) + \sqrt{2D_a}\mathrm{d}W_a(t). \tag{6.2c}$$

The corresponding Fokker-Planck equation is expressed by

$$\frac{\partial}{\partial t}P_{na}(v,t) = \nu(t)\left\{\frac{\partial}{\partial v}[\gamma v P_{na}(v,t)] + \frac{\partial^2}{\partial v^2}[(D_m v^2 + D_a)P_{na}(v,t)]\right\}. \tag{6.3}$$

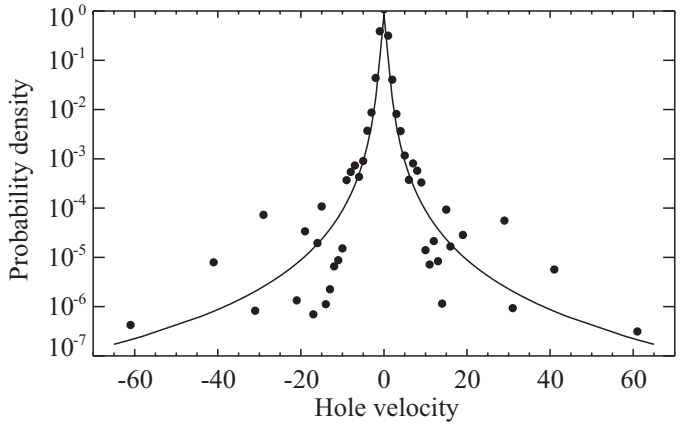

Figure 6.3: Probability distribution for hole velocity fluctuation. The black circles denote the probability distribution for the collected hole velocities with the help of the Rozenblatt-Parzen kernel density estimator. The solid line is the generalized Cauchy distribution with the estimated parameters by the maximum likelihood method as $a = 0.426$ and $b = 1.67$.

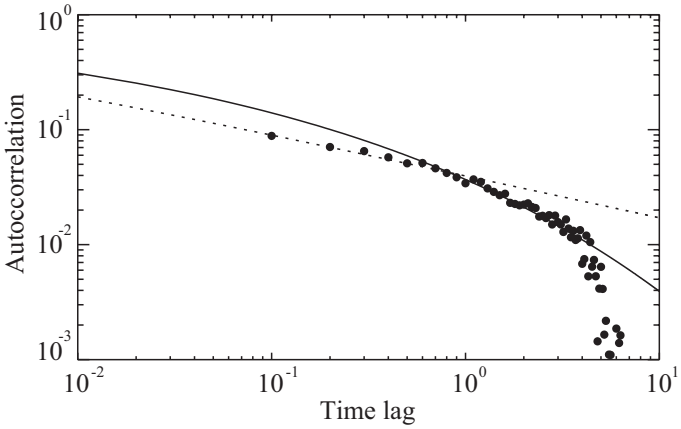

Figure 6.4: Autocorrelation coefficients of the hole velocity fluctuation denoted by the black circles. The solid line indicates the autocorrelation function of the NAGCP in Eq. (6.5) with its parameters $\gamma = 12.6$, $D_a = 3.96$, $D_m = 9.36$, and $\alpha = 0.75$. The dashed line indicates that of the FGCP in Eq. (6.8) with its parameters $\gamma = 67.2$, $D_a = 32.4$, $D_m = 49.9$, and $\beta = 0.37$.

and then gives its autocorrelation function in the form:

$$C_{na}(t) = \exp[-(\gamma - D_m)R(t)]. \tag{6.4}$$

Here a time-scaling function is given by $\nu(t) = (1-\alpha)t^{-\alpha}$ with $0 < \alpha < 1$ to incorporate the effect of long-memory, and then leads to $R(t) = t^{1-\alpha}$. In this case the autocorrelation function is given by a stretched exponential function,

$$C_{na}(t) = \exp[-(\gamma - D_m)t^{1-\alpha}], \tag{6.5}$$

as is denoted by the solid line in Fig. 6.4.

The other candidate is a fractional generalized Cauchy process (FGCP),

$$V_t^{fr} = X(S_t), \tag{6.6a}$$
$$S_t = \inf\{\tau; U_\alpha(\tau) > t\}, \tag{6.6b}$$
$$\mathrm{d}X(t) = -\gamma X(t)\mathrm{d}t + \sqrt{2D_m}X(t)\mathrm{d}W_m(t) + \sqrt{2D_a}\mathrm{d}W_a(t), \tag{6.6c}$$

with the corresponding fractional Fokker-Planck equation in the form:

$$\frac{\partial}{\partial t}P_{fr}(v,t) = {}_0\mathbf{D}_t^{1-\beta}\left\{\frac{\partial}{\partial v}[\gamma v P_{fr}(v,t)] + \frac{\partial^2}{\partial v^2}[(D_m v^2 + D_a)P_{fr}(v,t)]\right\}. \tag{6.7}$$

The autocorrelation function of this stochastic process is given by the Mittag-Leffler function [49] as

$$C_{fr}(t) = E_\beta[-(\gamma - D_m)t^\beta]. \tag{6.8}$$

which is also shown in Fig. 6.4 as the dashed line.

Both the NAGCP and the FGCP captures the characteristics of the probability distribution and the autocorrelation coefficients for the hole velocity fluctuation. In other words, it is necessary to get other statistical quantities such as higher order moments [42, 43], and structure functions [63] in order to determine the suitable stochastic process for the velocity fluctuation. Realizations of sample paths generated from numerical simulations [64] can also provide the information for specifying the appropriate stochastic model.

6.3 Summary

In this chapter, the kinetics of the hole velocities in the defect turbulence has been investigated. Firstly, the trajectory of each hole was displayed with its discrimination and then was subjected to be a kind of deterministic law. This observation requires the form of the coherent structures to have a time-dependent velocity term. The temporal variation of the hole velocity is caused by many body interactions between the local structures. Subsequently, we collected each hole velocity at cites in the space at each time and then regarded it as a time series data of the hole velocity fluctuation. The probability distribution for the hole velocity fluctuation displayed a symmetric unimodal shape with fat tails and was identified by the generalized Cauchy distribution. In addition, its autocorrelation coefficients exhibited non-exponential property, which implies the existence of long-memory. In

order to determine a stochastic process with the both characteristics, we employed the NAGCP and the FGCP. The both generalizations of the GCP capture the characteristics of the probability distribution and the autocorrelation coefficients of the velocity fluctuation. Thus, it is needed for specifying the suitable stochastic process to utilize other statistical quantities, such as higher-order moments, and structure functions, of the velocity fluctuation.

Chapter 7

Conclusions

7.1 Summary

In this dissertation, the defect turbulence of the 1D CGLE has been investigated from the point of view of the stochastic dynamics. For the purpose, the concept of the coherent structures, which are in the form of localized traveling waves, was introduced into the defect turbulence as the local structures. The local interactions between the local structures led to the birth-death process describing the stochastic dynamics in the defect turbulence.

In accordance with many previous works, the localized waves in the defect turbulence were discriminated based on only their amplitude values and named as LDW and LSW. The LDW number statistics displayed the sub-Poisson nature, which suggests the existence of the LDWs bunching states. Indeed, the evidence for this observation, as a sharp peak, was recognized in the probability distribution for inter-LDWs distance. Further, the probability distribution for depth of LDW was modeled by the Poisson process with long-range interactions.

The strict identification method for the local structures in the defect turbulence was introduced based on the information about their amplitude and phase, and then presented a defect, a hole, and an MAW as the local structures. The interaction scheme of the local structures was constructed and then led to the master equation, which was analytically solved with the help of independency of multi-variable Poisson distribution. This result is consistent with the observation for the numerical simulation where the marginal probability distribution for the number of each local structure is subjected to the Poisson distribution at the steady state. The validity of this identification was guaranteed by the probability distribution for inter-holes distance, where the sharp peak in the probability distribution for inter-LDWs distance was eliminated automatically. In other words, the sub-Poisson nature in the LDW number statistics with the LDWs bunching states is an unexpected illusion, which is caused by unsuitable identification of the localized waves.

In addition, interarrival time of defect, lifetime of holes, and that of MAWs were investigated. The probability distributions for them have the fat tails and the specific peaks, which implies that the birth-death process of the local structures is related to multi-time scale dynamics with long-memory. These effects were incorporated into the master equation as time-dependent functions in the form of the non-stationary master equation. The interarrival probability distribution function was analytically derived and gave good agreements with the probability distributions observed. It

is therefore concluded that the stochastic dynamics involved in the local structures in the defect turbulence can be completely modeled by the non-stationary master equation.

In analogy with the form of the coherent structures, the local structures were expected to travel with a constant velocity in the defect turbulence. However, the hole velocities observed displayed non-monotonic motions, namely the holes exhibited acceleration and/or deceleration depending on time, which may be caused by the interactions between the local structures. It is thus required that the velocity term in the form of the coherent structures is replaced by a time dependent function in generalizing them to more realistic cases with disorder.

The hole velocities without discrimination between the holes produced a time series data being regarded as the hole velocity fluctuation. The probability distribution for the hole velocity fluctuation was characterized by an unimodal shape with fat tails and thus was identified by the generalized Cauchy distribution. In addition, the autocorrelation coefficients exhibited a non-exponential decay, which implied the existence of long-memory. As the candidates describing the hole velocity fluctuation, the NAGCP and the FGCP were introduced. The autocorrelation functions of them indicated non-exponential features: the stretched exponential for the former, and the Mittag-Leffler function for the latter. These two generalizations of the GCP captures the characteristics of the probability distribution and autocorrelation coefficients of the hole velocity fluctuation.

These are our new findings among many investigations of the spatiotemporal dynamics of the CGLE after adopting the stochastic description in the defect turbulence. The theoretical method constructed here can be applied to other phenomena in nonequilibrium open systems.

7.2 Future prospects

In this dissertation, we have only focused on the defect turbulence while the 1D CGLE generates other types of spatiotemporal disorder such as phase turbulence and spatiotemporal intermittency. These dynamics can also be analyzed by non-stationary master equations derived from the interaction scheme of the local structures in the system.

From the point of view of the connection with real world, the 2D GCLE has to be studied. Previous researches in terms of statistical analysis for the 2D CGLE have only utilized topological defect as a localized nonlinear wave determining spatiotemporal dynamics. Likewise this study, local structures of the 2D CGLE have to be identified. However, the form of traveling wave cannot capture all the local structures of the 2D CGLE because the localized waves in 2D systems have rotational degrees of freedom in addition to translational degrees of freedom. Thus, as first step, the characteristics of localized waves of the 2D CGLE have to be investigated and then identification methods for them will have to be established to carry out an “appropriate” statistical analysis. This is a challenging task to understand the nature of nonequilibrium open systems.

Appendix A

Bloch's theorem

Here we consider the ensemble average $\langle \exp(X) \rangle$ with respect to the Gaussian distribution with a mean μ and a variance σ^2. This is calculated as

$$\begin{aligned} \langle \exp(X) \rangle &= \frac{1}{\sqrt{2\pi}} \int_{-\infty}^{\infty} \exp(x) \exp\left[-\frac{(x-\mu)^2}{2\sigma^2} \right] \mathrm{d}x \\ &= \exp\left(\frac{2\mu + \sigma^2}{2} \right) \frac{1}{\sqrt{2\pi}} \int_{-\infty}^{\infty} \exp\left[-\frac{(x-(\mu+\sigma^2))^2}{2\sigma^2} \right] \mathrm{d}x \\ &= \exp\left(\frac{2\mu + \sigma^2}{2} \right). \end{aligned} \tag{A.1}$$

This is known as the Bloch's theorem. In particular for a random variable $\sqrt{2D_m}W(t)$ being a Brownian motion with zero mean and variance $2D_m t$,

$$\langle \exp[\sqrt{2D_m}W(t)] \rangle = \exp(D_m t). \tag{A.2}$$

Appendix B

Derivation of the inverse Lévy transform

To begin with, we consider the generalized Fokker-Planck equation (GFPE) in multi dimensions,

$$\frac{\partial}{\partial t}P(\mathbf{r},t) = \int_0^t \mathrm{d}t' M(t-t') L_{FP} P(\mathbf{r},t'), \tag{B.1}$$

which is derived from the generalized master equation by the Kramers-Moyal expansion with the termination at the second term. The solution of the corresponding conventional Fokker-Planck equation,

$$\frac{\partial}{\partial t}p(\mathbf{r},t) = L_{FP} p(\mathbf{r},t), \tag{B.2}$$

provides that of the GFPE by an integral transform as

$$P(\mathbf{r},t) = \int_0^\infty p(\mathbf{r},\tau) K(\tau,t) \mathrm{d}\tau \tag{B.3}$$

with $K(\tau,t)$ being the integral kernel of which the Laplace transform with respect to t is given by

$$\hat{K}(\tau,s) = \frac{1}{s\hat{M}(s)} \exp\left[-\frac{\tau}{\hat{M}(s)}\right]. \tag{B.4}$$

Thus, the Laplace transform of $P(\mathbf{r},t)$ reads

$$\begin{aligned}
\hat{P}(\mathbf{r},s) &= \int_0^\infty \mathrm{d}t \mathrm{e}^{-st} \int_0^\infty \mathrm{d}\tau p(\mathbf{r},\tau) K(\tau,t) \\
&= \int_0^\infty \mathrm{d}\tau \frac{1}{s\hat{M}(s)} \exp\left[-\frac{\tau}{\hat{M}(s)}\right] p(\mathbf{r},\tau) \\
&= \frac{1}{s\hat{M}(s)} \hat{p}\left[\mathbf{r}, \frac{1}{\hat{M}(s)}\right].
\end{aligned} \tag{B.5}$$

The FFPE corresponds to the memory kernel having an asymptotic power-law behavior $M(t) \sim t^{-\alpha}$, of which the Laplace transform reads $\hat{M}(s) \sim s^{-\alpha}$. Therefore, Eq. (B.5) leads to the formula

$$\hat{P}(\mathbf{r},s) = s^{\alpha-1} \hat{p}(\mathbf{r}, s^\alpha). \tag{B.6}$$

Appendix C

The sample paths corresponding to the FFPE

Here, we consider the following stochastic processes system:

$$Y_t = X(S_t), \tag{C.1}$$
$$S_t = \inf\{\tau; U_\alpha(\tau) > t\}, \tag{C.2}$$
$$\mathrm{d}X = F(X)\mathrm{d}\tau + G(X)\mathrm{d}W(\tau). \tag{C.3}$$

The characteristic function of the PDF of the strictly increasing α-stable Lévy process $U_\alpha(\tau)$ [38] is given by the Laplace transform as

$$\begin{aligned} \hat{u}(s,\tau) &= \int_0^\infty u(t,\tau)\mathrm{e}^{-st}\mathrm{d}t \\ &= \exp(-\tau s^\alpha). \end{aligned} \tag{C.4}$$

This characteristic function satisfies

$$\hat{u}(s,\tau) = \hat{u}(\tau^{1/\alpha}s) \tag{C.5}$$

with $u(t) = u(t,1)$. This relations leads to

$$\begin{aligned} \int_0^\infty u(t,\tau)\mathrm{e}^{-st}\mathrm{d}t &= \int_0^\infty u(t')\mathrm{e}^{-\tau^{1/\alpha}st'}\mathrm{d}t' \\ &= \int_0^\infty \frac{1}{\tau^{1/\alpha}} u\left(\frac{t}{\tau^{1/\alpha}}\right)\mathrm{e}^{-st}\mathrm{d}t. \end{aligned} \tag{C.6}$$

Thus, we obtain the $1/\alpha$ self-similar scaling relation

$$u(t,\tau) = \frac{1}{\tau^{1/\alpha}} u\left(\frac{t}{\tau^{1/\alpha}}\right). \tag{C.7}$$

The definition of $\{S_t\}_{t\geq 0}$ gives

$$\mathrm{Prob}(S_t < \tau) = \int_0^\tau g(\tau', t)\mathrm{d}\tau = \int_t^\infty u(t', \tau)\mathrm{d}t' = \mathrm{Prob}(U(\tau)\geq t), \tag{C.8}$$

where $g(\tau, t)$ is the PDF of $\{S_t\}_{t\geq 0}$. Derivative with respect to τ for both sides in Eq. (C.8) leads to

$$\begin{aligned} g(\tau,t) &= \frac{\partial}{\partial\tau}\int_t^\infty u(t',\tau)\mathrm{d}t' \\ &= \frac{\partial}{\partial\tau}\int_t^\infty \frac{1}{\tau^{1/\alpha}}u\left(\frac{t'}{\tau^{1/\alpha}}\right)\mathrm{d}t' \\ &= \frac{\partial}{\partial\tau}\int_{t/\tau^{1/\alpha}}^\infty u(t'')\mathrm{d}t'' \\ &= \frac{t}{\alpha\tau^{1+1/\alpha}}u\left(\frac{t}{\tau^{1/\alpha}}\right) \\ &= \frac{t}{\alpha\tau}u(t,\tau). \end{aligned} \tag{C.9}$$

This gives the Laplace transform of $g(\tau, t)$ with respect to t as

$$\begin{aligned} \hat{g}(\tau,s) &= \int_0^\infty g(\tau,t)\mathrm{e}^{-st}\mathrm{d}t \\ &= \int_0^\infty \frac{t}{\alpha\tau}u(t,\tau)\mathrm{e}^{-st}\mathrm{d}t \\ &= -\frac{1}{\alpha\tau}\frac{\partial}{\partial s}\int_0^\infty u(t)\mathrm{e}^{-st}\mathrm{d}t \\ &= -\frac{1}{\alpha\tau}\frac{\partial}{\partial s}\exp(-\tau s^\alpha) \\ &= s^{\alpha-1}\exp(-\tau s^\alpha). \end{aligned} \tag{C.10}$$

Assume that $\{X(\tau)\}_{\tau\geq 0}$ and $\{S_t\}_{t\geq 0}$ are independent stochastic processes, we obtain

$$P(x,t) = \int_0^\infty p(x,\tau)g(\tau,t)\mathrm{d}\tau, \tag{C.11}$$

where $P(x, t)$ and $p(x, \tau)$ are the PDF of $\{Y_t\}_{t\geq 0}$ and $\{X(\tau)\}_{\tau\geq 0}$, respectively. The Laplace transform of Eq. (C.11) with Eq. (C.10) leads to

$$\begin{aligned} \hat{P}(x,s) &= \int_0^\infty P(x,t)\mathrm{e}^{-st}\mathrm{d}t \\ &= \int_0^\infty p(x,\tau)\hat{g}(\tau,s)\mathrm{d}\tau \\ &= \int_0^\infty p(x,\tau)s^{\alpha-1}\exp(-\tau s^\alpha)\mathrm{d}\tau \\ &= s^{\alpha-1}\hat{p}(x,s^\alpha). \end{aligned} \tag{C.12}$$

This is the same relation in Eq. (B.6). It is therefore proven that $\{Y_t\}_{t\geq 0}$ is the stochastic process corresponding to the FFPE.

Appendix D

The solution of the non-stationary master equation

Here we consider the non-stationary mater equation in the form:

$$\frac{\mathrm{d}}{\mathrm{d}t}P(n;t) = (1+\psi(t))\nu(t)[P(n-1;t) - P(n;t)] + \nu(t)[(n+1)P(n+1;t) - nP(n;t)] \quad \text{(D.1)}$$

with the restrictions that $\nu(t)$ must be positive, and $\psi(t)$ is integrable. Introduced a rescaled time

$$\tau = \int_0^t \nu(t')\mathrm{d}t', \quad \text{(D.2)}$$

Eq. (D.1) leads to

$$\frac{\mathrm{d}}{\mathrm{d}\tau}P(n;\tau) = (1+\psi(\tau))[P(n-1;\tau) - P(n;\tau)] + [(n+1)P(n+1;\tau) - nP(n;\tau)]. \quad \text{(D.3)}$$

The generating function [42, 43] defined by

$$g(z,\tau) = \sum_0^\infty z^n(\tau)P(n;\tau) \quad \text{(D.4)}$$

with Eq. (D.3) gives the evolution equation in the form:

$$\frac{\partial}{\partial\tau}g(z,\tau) + (z-1)\frac{\partial}{\partial z}g(z,\tau) = (1+\psi(\tau))g(z,\tau). \quad \text{(D.5)}$$

This equation is a first order partial differential equation and then can be solved by the method of characteristics [65]. Characteristic equations of Eq. (D.5) are given by

$$\frac{\mathrm{d}\tau}{1} = \frac{\mathrm{d}z}{z-1} = \frac{\mathrm{d}g}{(1+\psi(\tau))(z-1)g}. \quad \text{(D.6)}$$

The equation with respect to the first equality gives the evolution of $z(\tau)$ by

$$z(\tau) = [z_0 - 1]\mathrm{e}^\tau, \quad \text{(D.7)}$$

with z_0 being an initial value of $z(\tau)$. Then the second one gives

$$g(z,\tau) = g(z_0,0)\exp\left[\int_0^\tau (1+\psi(\tau'))(z(\tau')-1)\mathrm{d}\tau'\right], \tag{D.8}$$

where the specific form of $g(z_0,0)$ is determined by an initial probability distribution $P(n;0)$. When the initial distribution is given by the Kronecker delta as $P(n;0)=\delta_{n,0}$, Eq. (D.8) leads to

$$g(z,\tau) = \exp[-\Phi(\tau)]\exp[\Phi(\tau)z] \tag{D.9}$$

with

$$\Phi(\tau) = \mathrm{e}^{-\tau}\int_0^\tau (1+\psi(\tau'))\mathrm{e}^{\tau'}\mathrm{d}\tau'. \tag{D.10}$$

With the definition of the generating function, $g(z,\tau)$ is also written by

$$g(z,\tau) = \exp[-\Phi(\tau)]\sum_0^\infty \frac{[\Phi(\tau)]^n}{n!}z^n. \tag{D.11}$$

Then $P(n;\tau)$ is readily obtained by

$$P(n;\tau) = \frac{[\Phi(\tau)]^n}{n!}\exp[-\Phi(\tau)]. \tag{D.12}$$

Substituting Eq. (D.2) into Eq. (D.12), one can obtain the solution of the original non-stationary master equation in Eq. (D.1).

References

[1] M. C. Cross and P. C. Hohenberg, Rev. Mod. Phys. **65**, 851 (1993).

[2] M. Cross and H. Greenside, *Pattern Formation and Dynamics in Nonequilibrium Systems*, Cambridge University Press, 2009.

[3] J. Lega, B. Janiaud, S. Jucquois, and V. Croquette, Phys. Rev. A **45**, 5596 (1992).

[4] J. M. Flesselles, V. Croquette, and S. Jucquois, Phys. Rev. Lett. **72**, 2871 (1994).

[5] B. P. Belousov, Coll. Abs. Rad. Med. [in Russian] **147**, 145 (1959).

[6] A. M. Zhabotinsky, Biophys. [in Russian] **9** 306 (1964).

[7] T. Frisch, S. Rica, P. Coullet, and J. M. Gilli, Phys. Rev. Lett. **72**, 1471 (1994).

[8] I. Aranson, Phys. Rev. E, **51**, R3827 (1995).

[9] A. Pertsov, J. M. Davidenko, Remy Salomonsz, W. T. Baxter, and J. Jalife, Circ. Res. **72**, 631 (1992).

[10] A. S. Orovio, E. M. Cherry, and F. H. Fenton, J. Theor. Biol. **253**, 544 (2008).

[11] R. H. Clayton, *et. al.*, Prog. Biophys. Molec. Biol. **104**, 22 (2011).

[12] H. Lamb, *Hydrodynamics*, Cambridge University Press, 1895.

[13] A. H. Nayfeh, *Perturbation Methods*, Wiley, 1973.

[14] J. D. Gibbon, and M. J. Mcguiness, Proc. R. Soc. Lond. A **377**, 185 (1981).

[15] T. Taniuchi, Prog. Theor. Phys. Suppl. **9**, 69 (1959).

[16] Y. Kuramoto, *Chemical Oscillations, Waves, and Turbulence*, Dover, New York, 2003.

[17] I. S. Aranson, and L. Kramer, Rev. Mod. Phys. **74**, 99.

[18] L. Gil, J. Lega, and J. L. Meunier, Phys. Rev. A **41**, 1138 (1990).

[19] C. Beta, A. S. Mikhailov, H. H. Rotermund, and G. Ertl, Europhys. Lett. **75**, 868 (2006).

[20] K. E. Daniels, and E. Bodenschatz, Chaos **13**, 55 (2003).

[21] A. Suzuki, and H. Konno, AIP Adcances **1**, 032103 (2011).

[22] N. Bekki, Y. Harada, and H. Kanai, J. Phys. Soc. Jpn. **81**, 073801 (2012).

[23] K. Nozaki, and N. Bekki, J. Phys. Soc. Jpn., **53**, 1681 (1984).

[24] J. Lega, Physica D **152**-**153**, 269 (2001).

[25] S. Popp, O. Stiller, I. Aranson, A. Weber, and L. Kramer, Phys. Rev. Lett. **70**, 3880 (1993).

[26] P. S. Hagan, SIAM J. Appl. Math. **42**, 762 (1982).

[27] I. S. Aranson, A. R. Bishop, and L. Kramer, Phys. Rev. E **57**, 5276 (1998).

[28] W. van Saarloos, and P. C. Hohenberg, Physica D, **56**, 303 (1992), Physica D **69**, 209 (1993).

[29] M. van Hecke, Phys. Rev. Lett. **80**, 1896 (1998).

[30] L. Brucsh, M. Zimmermann, M. van Hecke, M. B är, and A. Torcini, Phys. Rev. Lett. **85**, 86 (2000).

[31] H. Chaté, Nonlinearity **7**, 185 (1994).

[32] J. A. Sherratt, and M. J. Smith, Physica D **241**, 1671 (2012).

[33] M. van Hecke, and M. Howard, Phys. Rev. Lett. **86**, 2018 (2001).

[34] H. Sakaguchi, Phys. Rev. E **76**, 017205 (2007).

[35] H. Wang, Phys. Rev. Lett., **93**, 154101 (2004).

[36] L. Arnold, *Random Dynamical Systems*, Springer, 1998.

[37] K. E. Daniels, C. Beck, and E. Bodenschatz, Physica D **193**, 208.

[38] A. Janicki, and A. Weron, *Simulation and Chaotic Behavior of α-Stable Stochastic Processes*, Marcel Dekker, New York, 1994.

[39] H. Sakaguchi, J. Phys. Soc. Jpn. **70**, 3247 (2001).

[40] H. Konno, and F. Watanabe, J. Math. Phys. **48**, 103303 (2007).

[41] I. Lubaschevsky, R. Friedrich, and A. Heuer, Phys. Rev. E **79**, 01110 (2009).

[42] C. Gardiner, *Stochastic Methods: A Handbook for the Natural and Social Sciences*, Springer-Verlag, Berlin, 2009.

[43] N. G. van Kampen, Stochastic Processes in Physics and Chemistry, Elsevier, Amsterdam, 2007.

[44] T. Bedford, and R. Cooke, *Probabilistic Risk Analysis: Foundations and Methods*, Cambridge University Press, 2001.

[45] H. Konno, Adv. Math. Phys. **2010**, 504267 (2010).

[46] E. W. Montroll, G. H. Weiss, J. Math. Phys. **9**, 167 (1965).

[47] R. Metzler, and J. Klafter, Phys. Pep. **339**, 1 (2000).

[48] J. Klafter, and I. M. Sokolov, *First Steps in Random Walks*, Oxford University Press, 2011.

[49] I. Podlubny, *Fractional Differential Equations*, Academic press, 1999.

[50] A. Pirytinska, A.I. Saichev, and W. A. Woyczynski, Physica A **349**, 375 (2005).

[51] A. A. Stanislavsky, Phys. Rev. E **67**, 021111 (2003).

[52] M. Magdziarz, A. Weron, and K. Weron, Phys. Rev. E **75**, 016708 (2007).

[53] J. B. Gonpe Tafo, L. Nana, and T. C. Kofane, Phys. Rev. E **88**, 032911.

[54] H. Haken, *Light: Volume 1: Waves, Photons, Atoms*, North Holland, 1981, *Light: Volume 2: Laser Light Dynamics*, North Holland, 1986.

[55] Y. Kuramoto, Prog. Theor. Phys. **49**, 1782 (1973).

[56] H. Konno, and P. S. Lomdahl, J. Phys. Soc. Jpn. **69**, 1629 (2000).

[57] F. W. J. Oliver, D. W. Lozier, R. F. Boisvert, and C. W. Clark, *NIST Handbook of Mathematical Functions*, Cambridge University Press, 2010.

[58] C. Beck, and E. G. D. Cohen, Physica A **322**, 267 (2003).

[59] E. Orsingher, and F. Polito, Stat. Prob. Lett. **82**, 852 (2012).

[60] M. van Hecke, Physica D **174**, 134 (2003).

[61] M. Howard, and M. van Hecke, Phys. Rev. E **68**, 02613 (2003).

[62] L. Brucsh, A. Torcini, M. van Hecke, M. G. Zimmermann, and M. Bär, Physica D **160**, 127 (2001).

[63] N. Mordant, P. Metz, O. Michel, and J.-F. Pinton, Phys. Rev. Lett. **87**, 214501 (2001).

[64] J. R. Klauder, and W. P. Petersen, SIAM J. Numer. Anal. **22**, 1153 (1985).

[65] S. J. Farlow, *Partial Differential Equations for Scientists and Engineers*, Dover, 1993.

Publications

Reviewed journal papers

[J1] Y. Uchiyama, and H. Konno, Phys. Lett. A **378**, 1350 (2014).
[J2] Y. Uchiyama, and H. Konno, Int. J. Phys. Natur. Sci. Eng. **7**, 20 (2013).

Reviewed conference proceedings

[C1] Y. Uchiyama, and H. Konno, *20th Australian Physics Congress*, New South Wales, Australia, Dec. 9–10, 2012, No. 303.
[C2] Y. Uchiyama, and H. Konno, *45th ISCIE International Symposium on Stochastic Systems Theory and Its Applications*, Okinawa, Japan, Nov. 1–2, 2013 (to appear).
[C3] H. Konno, and Y. Uchiyama, *44th ISCIE International Symposium on Stochastic Systems Theory and Its Applications*, Tokyo, Japan, Nov. 1–2, 2012, 180 (2012).

Acknowledgement

I wish to express my sincere gratitude to the following people.

First and foremost I would like to express my gratitude to my supervisor, Prof. Hidetoshi Konno for welcoming me to his Lab. and for his guidance throughout my studies with his unsurpassed knowledge of complex systems. I appreciate him taking time from his busy schedule to discuss my studies and suggesting me improvement of quality. From his attitude toward understanding nature in complex real systems, I have learned a lot. Someday I would like to catch up his standing and to get over his achievements as his pupil.

I am very grateful to Prof. Hiroshi Yabuno for introducing me to the world of nonlinear dynamics when I was an undergraduate student. A part of this dissertation is supported by his initiation into some techniques of the nonlinear dynamics.

I am very grateful to my co-advisors Prof. Harumichi Kyoto and Assoc. prof. Yuko Hatano for giving comments for developing my ability as a researcher.

I am very grateful to Prof. Yasuhiro Hatsugai for making advices on this dissertation to enable me to organize it effectively.

I am oblige to the members of Prof. Konno's Lab. and Assoc. prof. Hatano's Lab. for making my academic life confortable. In particular, I am grateful to Shun Fukuchi for giving his knowledge of anomalous diffusion and fractional calculus, and to Takanori Kadoya for taking his insight into stochastic processes with long-memory. Without their supports, some parts of this dissertation could not be accomplished.

I am deeply grateful to my ex-bosses, Tomoji Watanabe, Masayuki Kaiho, Takahiro Nishioka, Shigehisa Funabashi, Masanori Watanebe, Taku Iwase, Tadayuki Sato, and the menbers of 1st Dept. for giving my career as an engineer. The experiences of developing products have helped me investigate complex real products. Particularly to Takeshi Honda, I am very grateful, for having taught me the importance of investigating the essences of phenomena again and again.

I am also deeply grateful to Akio Idei, Shigemasa Satoh, Shigeyasu Tsubaki, and the members of Engineering Technology Development Department for encouraging me to go to Ph. D. course. I am especially grateful to Akira Gotoh for cheering me up night and day, and for giving deep insights to engineering.

I would like to thank my friends and ex-colleagues for their support. Akira Ohshima shows me his attitude to catch his dream, which always stimulate my mind. Sota Kimura encourages me to go on studying complex systems with his insight to fracture mechanics, and to become a "true" researcher. Norihito Kobata is my best teacher of numerical simulation. Without his lessons in the M2 building, I could not carry out the numerical simulations in this dissertation. I will tend to collaborate with them in their fields in years to come. Tjedrk Jan VREEKEN looked over a paper

before submitting. Yuji Asai and Shinsuke Iwashita gave me a jolt when I was eighteen years old, which is my origin in retrospect. Rina Hanagaki, Aino Kishi, and Kaho Kasumi reminded me of the importance of challenging by showing their attitude toward their life.

Finally, I am very grateful to Japan Society for the Promotion of Science (JSPS) for my research by Grant-in-Aid for JSPS Fellows No. 25.374.